Medizinische Fakultät
der
Universität Duisburg-Essen

Aus dem Institut für Zellbiologie (Tumorforschung)

Exploiting drug-induced HR-ness for synthetic lethality in combination with radiotherapy

Inauguraldissertation
zur
Erlangung des Doktorgrades der Medizin
durch die Medizinische Fakultät
der Universität Duisburg-Essen

Vorgelegt von
Kexu Xiang
Aus Sichuan, P.R. China
2021

DuEPublico
Duisburg-Essen Publications online

UNIVERSITÄT DUISBURG ESSEN
Offen im Denken

ub universitäts bibliothek

Diese Dissertation wird via DuEPublico, dem Dokumenten- und Publikationsserver der Universität Duisburg-Essen, zur Verfügung gestellt und liegt auch als Print-Version vor.

DOI: 10.17185/duepublico/76235
URN: urn:nbn:de:hbz:465-20220824-090013-0

Alle Rechte vorbehalten.

Dekan: Herr Univ.-Prof. Dr. med. J. Buer

1. Gutachter/in: Frau Univ.-Prof. Dr. rer. nat. V. Jendrossek

2. Gutachter/in: Frau Univ.-Prof. Dr. phil. nat. K. Lückerath

Tag der mündlichen Prüfung: 10. Juni 2022

Included in this dissertation is the following original review:

Xiang K, Jendrossek V, Matschke J. Oncometabolites and the response to radiotherapy. Radiat Oncol. 2020 Aug 14;15(1):197. doi: 10.1186/s13014-020-01638-9. PMID: 32799884; PMCID: PMC7429799.

and a manuscript as an original work with Kexu Xiang as a first author in revision process:

Xiang K. Kalthoff C, Münch C, Jendrossek, Matschke J. Accumulation of oncometabolite D-2-Hydroxyglutarate by SLC25A1 inhibition: a metabolic strategy for induction of HR-ness and radiosensitivity. Cell Death & Disease (in revision).

Contents

1 Introduction

1.1 Cancer is a major burden for humankind

Cancer is characterized as an abnormal phenomenon in which cells grow uncontrollably to invade surrounding tissue and distribute to other parts of the body. According to estimates from the World Health Organization (WHO) in 2019, cancer is the first or second leading cause of death before the age of 70 years in 112 out of 183 countries in the world (Figure 1) (Sung et al., 2021). Although different countries exhibit different epidemiology distribution of cancer incidence and mortality, the rapid growing burden of the malignant disease has set an obstacle to improve life quality in the whole world. There were an estimated 19.3 million new cases (18.1 million excluding non-melanoma skin cancer, except basal cell carcinoma) and 10 million cancer deaths (9.9 million excluding non-melanoma skin cancer, except basal cell carcinoma) worldwide in 2020 (Sung *et al.*, 2021). The epidemiology data shows that the distribution of cancer is closely related with gender, Human Development Index (HDI), and geographic position. The top ten cancer types account for >60% of the newly diagnosed cases and >70% of the cancer deaths. Female breast cancer is the most commonly diagnosed cancer (11.7% of total cases) and lung cancer is the primary cause of cancer death (18.0% of the total cancer deaths) (Sung *et al.*, 2021). Lung cancer is the most frequently occurring cancer among all cancers and the leading cause of cancer death in men, followed by prostate and colorectal cancer for incidence and liver and colorectal cancer for mortality (Sung *et al.*, 2021). In women, breast cancer is the most diagnosed cancer and the leading cause of cancer death, followed by colorectal and lung cancer for incidence and mortality (Sung *et al.*, 2021). Furthermore, recent statistics of new cancer cases in 2020 estimated lung cancer with 2.2 million new cancer cases as the second most diagnosed cancer and with 1.8 million deaths, even the leading cancer with high mortality rate (Sung *et al.*, 2021). The survival of patients with lung cancer at 5 years after diagnosis is only 10% to 20% in most countries among those diagnosed during 2010-2014 (Sung *et al.*, 2021). Glioblastoma, with a high risk and recurrence, is the one of the leading causes of central nervous system cancer, and only fewer than 3–7% of patients surviving longer than five years (McNeill, 2016).

With the prolongation of human life span and growing proportion of middle-aged and elderly people, the world witnesses increasing cancer new cases and death rates, it is demanding to develop efficient weapons to fight against this cluster of disease.

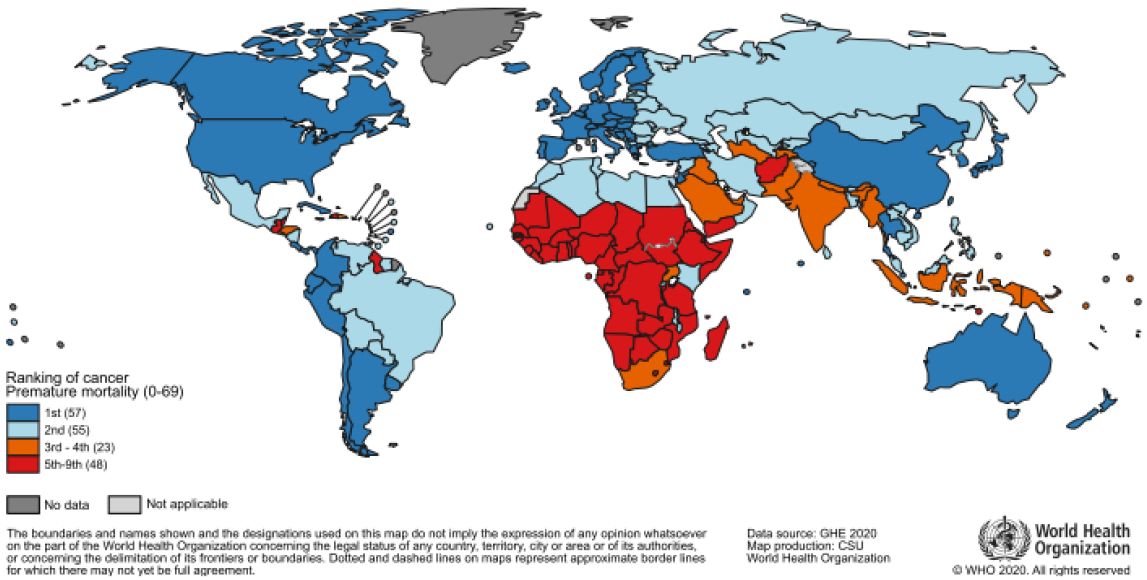

Figure 1: Global Cancer Statistics 2020: National Ranking of Cancer as a Cause of Death at Ages <70 Years in 2019 (Sung *et al.*, 2021).

1.2 Radiotherapy and its main challenges

Treatments for cancer imply multimodal therapies and are composed of RT, chemotherapy, immunotherapy, surgery, or combination of therapies to prevent cancerous spread and to induce local elimination. Radiotherapy (RT) is commonly used to treat cancer, especially solid tumors. The local application of ionizing radiation (IR) to target and kill cancer cells with high precision has been shown to be beneficial for local control, overall survival and cure rates for various tumor types. The strategy of RT is high accuracy of radiation towards cancerous tumor and protection of surrounding normal tissue, in the purpose of permanent control, extended survival time of patients and the improvement of the life quality. Indeed, the therapeutic potential of RT alone and in multimodal combinations with chemotherapy, surgery and targeted drug therapy has increased substantially in the last decades (Kirsch et al., 2018). Nevertheless, progressive cancers are characterized by significant radioresistance, leading to local recurrence, and co-irradiation of normal tissues may lead to toxicity, thus limiting the use of maximum

applicable RT dose. The risk of adverse effects also limits efforts to enhance treatment by combining RT with any other cancer treatment, RT dose escalation. As a result, local recurrence and distant metastases from the primary tumor remain a major cause of death in many cancer patients (reviewed by Xiang et al., 2020).

RT is widely used as a standard treatment option due to its ability to disrupt cellular macromolecules thus effectively inducing growth arrest and death of irradiated tumor cells (Abshire and Lang, 2018). Exposure to IR directly promotes DNA damage or indirectly induces the production of reactive oxygen species (ROS) (Li et al., 2019). Nevertheless, the high intrinsic, microenvironment-mediated and adaptive radioresistance of human solid tumors remain major obstacles to execute efficacious RT. For instance, the cytotoxic efficacy of RT depends on the local availability of molecular oxygen (O_2) in the tumor tissue during treatment to generate ROS and to fix RT-induced DNA damage (56). Thus, an acute and severe decrease in O_2 level ("tumor hypoxia") due to insufficient O_2 supply, increased O_2 demand, or both, can promote direct resistance by reducing oxidative stress and treatment-induced cell death (Bristow and Hill, 2008; reviewed by Xiang *et al.*, 2020).

DNA double-strand break (DSB) is one of the common forms of IR-induced DNA damage, disrupting DNA structure and triggering cell death. In fact, DNA DSBs are considered as the most toxic lesions. Despite that, DSBs can also induce a range of DNA damage responses (DDRs), including activation of DNA damage detecting and early transduction pathways, cell cycle arrest and DNA repair, to help these cells escape genomic instability and to recover from radiation damage. These DDRs play an important role in radiation resistance. In addition to DDR, the mechanisms that may lead to radioresistance are as follows: a) Altered tumour microenvironment (TME). This process includes remodelling of hypoxic conditions, cytokine levels and overproduction of metabolites (Hinshaw and Shevde, 2019); b) Induction of autophagy. Autophagy protects damaged organelles in a manner that maintains metabolic, energy and redox homeostasis. Autophagy can also increase the stability of chromosomes or genomes to counteract the effects of radiation (Mizushima and Levine, 2020); c) Tumour metabolism. Changes in mitochondrial metabolism and modifications in glycolysis are associated with radiation resistance(Floberg and Schwarz, 2019); d) Cell cycle arrest. Stagnation of cancer cells in the G2/M phase has been verified to be associated with the development of

radioresistance (Li et al., 2013); e) Cancer stem cells (CSCs). CSCs are a subpopulation of cancer cells that can drive cancer origination or recurrence. CSCs are sensitive to DNA damage response and ROS clearance, thus leading to radioresistance. In addition, CSCs can activate the IGF1-AKT signalling pathway to promote radioresistance (Li et al., 2016). Important molecular determinants of intrinsic and acquired radioresistance are: a) the ability of cells to detoxify radiation-induced ROS; and b) the ability to efficiently repair RT-induced DNA damage, especially for the most lethal DSBs (Roos et al., 2016). Although DSBs represent only a small proportion of RT-induced DNA damage, they impose a great challenge for the cell. Therefore, cells have developed various mechanisms to ensure survival, which include different DSB repair pathways such as non-homologous end joining (NHEJ), homologous recombination repair (HRR) or alternative end joining (alt-EJ) (Mladenov and Iliakis, 2011). Thus, genetic abnormalities that enhance the ability of cancer cells to undergo DSB repair via NHEJ, HRR or alt-EJ may promote survival of cancer cells exposed to genotoxic therapies and enhance radiation resistance (Matschke et al., 2016a; reviewed by Xiang *et al.*, 2020). Conversely, genetic abnormalities leading to defects in DDR and DNA DSB repair pathways, such as early onset breast cancer 1/2 (BRCA1/2), enhance susceptibility to DNA damage therapies, such as chemotherapy and RT. Hence, these genetic alterations may create specific vulnerability to inhibitors of complementary DSB repair pathway to achieve so-called synthetic lethality (reviewed by Xiang *et al.*, 2020).

Intriguingly, emerging evidence suggests that in addition to genetic defects in DDR and DSB repair core proteins, other factors such as microenvironmental cues (Bristow and Hill, 2008), metabolic enzymes or dysregulation of the expression or mutation of chromatin modifiers (Hlouschek et al., 2018a; Matschke *et al.*, 2016a) can also promote DSB repair defects in cancer cells, with important therapeutic implications. Furthermore, the ability of cancer cells to maintain cellular redox homeostasis and high antioxidant capacity, as part of metabolic reprogramming during malignancy development, is associated with radioresistance (Hlouschek *et al.*, 2018a; Hlouschek et al., 2018b; Matschke *et al.*, 2016a). Finally, metabolic adaptation of cancer cells to unfavourable conditions in the tumor microenvironment or to treatment-induced stress can promote acquired radioresistance and provide additional targets for tumor-specific radiosensitization (Hlouschek *et al.*, 2018a; Hlouschek *et al.*, 2018b; Matschke *et al.*,

2016a; Matschke et al., 2016b). However, a caveat to the use of metabolic inhibitors in cancer therapy remains the great molecular heterogeneity within and between different tumors, highlighting the necessity and urgency of developing reliable biomarkers for patient stratification.

1.3 Cancer metabolic rewiring

During and after the transformation to cancerous states, cells tend to rewire cellular metabolism to satisfy the growing demands of cell growth and proliferation. Due to the diversity of metabolic changes within the metabolic program of a cancer cell, it is not possible to apply an accurate single model of altered tumor metabolism to describe the overall state of metabolic changes which support cancerous cell growth (4). It is worth noting that cancer cell metabolism is based on influences of the tumour microenvironment and the distance to the vasculature. Cancer cells which are closer to the blood supply can profit from their access to nutrients and oxygen, thus generating ATP aerobically via oxidative phosphorylation and upregulating anabolic pathways, to support rapid proliferation (Viallard and Larrivee, 2017). For cancer cells which locate far from vasculature, tend to commit to alternative catabolic metabolic pathways due to low nutrient availability (Brahimi-Horn et al., 2007). For energy supplementation, most tumor cells utilize glucose, lactate, pyruvate, hydroxybutyrate, acetate, acetoacetate, glutamine and free fatty acid at much higher rates than their non-tumor counterparts as bioenergetic support for tumor growth. Furthermore, cancer cells can benefit from surrounding cancer or stromal cells for their growth. For instance, cervical cancer and colon cancer models have revealed that hypoxic cancer cells, which preferentially metabolize glucose anaerobically via glycolysis to produce lactate, are metabolically coupled to other normoxic cancer cells. These normoxic cancer cells mainly utilize lactate as a substrate for mitochondrial oxidative phosphorylation (OXPHOS) (Martinez-Outschoorn et al., 2017). Anabolic pathways, which provide building blocks for cancer cells, are under transformation during malignant process. The metabolism of serine and glycine provides one-carbon units which can be used to produce nucleotides. Phosphoglycerate dehydrogenase (PHGDH), which catalyses serine biosynthesis from 3-phosphoglycerate, has been shown to maintain the oncogenic potential of breast cancer and melanoma cell (Locasale et al., 2011). During the rapid proliferation of cancer cells, lipids and steroids are necessary components to form phospholipid bilayers for cell division. It has been

discovered that several enzymes are involved in these pathways, including fatty acid synthase, ATP citrate lyase, acetyl-CoA carboxylase, mono glyceride lipase HMG-CoA reductase (HMGCR), and choline kinases are associated with tumour development and progression *in vitro* and *in vivo* (Flavin et al., 2010).

Mitochondria provide cells with energy, materials for structure construction. Functional analysis shows that mitochondria regulate cell activity through both, modification of redox homeostasis and oncogenic signals (Frezza, 2014).

One theory of energy production for cancer cells was based on the observation of Otto Warburg that cancer cells acquire the unusual property of taking up and applying glucose to lactate production in spite of sufficient oxygen presence (aerobic glycolysis). He proposed that defects in mitochondrial respiration are the underlying basis for aerobic glycolysis in cancer cells ("Warburg effect") (Warburg, 1956). However, Fantin and colleagues provided evidence that most tumor mitochondria are not defective in their ability to carry out oxidative phosphorylation and cancer cells had substantial reserve capacity to produce ATP by OXPHOS (Fantin et al., Cancer Cell 2006).

Furthermore, discovery about the energy source of tumor cells has revealed that glutamine, instead of glucose, is taken up by the cancer cells at higher levels than any other metabolite in some tumors (Reinfeld et al., 2021). This corroborates that aerobic glycolysis is not the only metabolic pattern of cancer cells. Moreover, tumor cells are able to replenish OXPHOS and TCA cycle employing glutaminolysis, pyruvate carboxylation and so on (DeBerardinis et al., 2007). Particularly, glutaminolysis provides TCA cycle with α-ketoglutarate which undergoes reductive carboxylation, producing citrate and acetyl-CoA which can be used for fatty acid synthesis (Mullen et al., 2011). In addition, amino acids, nucleotides, as well as redox-balancing metabolites, such as nicotinamide adenine dinucleotide phosphate reduced (NADPH), can also be the products of synthesis process of mitochondria (Cantor and Sabatini, 2012).

As the power source and nutrition supplier of a cell, mitochondria also contribute to and endure transformation in cancer cells for their role in ROS generation (Jezek et al., 2018). Mitochondrial DNA mutations exert influence on a variety of electron transport chain (ETC) as they promote ROS generation in tumors (Shadel and Horvath, 2015). ROS are a cluster of species that can be produced in all cells as a normal by-product of metabolic

processes. ROS characterise as heterogeneous in their properties and could lead to abundant downstream effects, depending on the concentrations in cells (Giannoni et al., 2005). At low levels, ROS increase cell survival and proliferation through the post-translational modification of kinases and phosphatases, thus regulating the process of tumor generation (Giannoni *et al.*, 2005). At moderate levels, ROS can give rise to the expression of stress-responsive genes such as HIF1A, which in turn trigger the expression of proteins which provide pro-survival signals, such as the glucose transporter GLUT1, also known as SLC2A1, and vascular endothelial growth factor (VEGF) (Gao et al., 2007; Takahashi et al., 2006). What's more, at high levels, ROS can induce the activation of protein kinase Cδ (PKCδ) or MAP kinase signalling to activate downstream effects (Shadel and Horvath, 2015), or damage macromolecules of cell, such as DNA, trigger senescence, and increase permeability of the mitochondria, leading to the release of cytochrome c and apoptosis (Figure 2). Moreover, ROS, as well as cathepsins, plays important role in the process of cell apoptosis and death in the way of lysosomal membrane permeabilization (Martinez-Carreres et al., 2017).

Thus, in fast growing and proliferating cancer cells, detoxification of ROS is important because oncogenic mutations promote aberrant metabolism and protein production which lead to increased ROS production(DeBerardinis and Chandel, 2016).

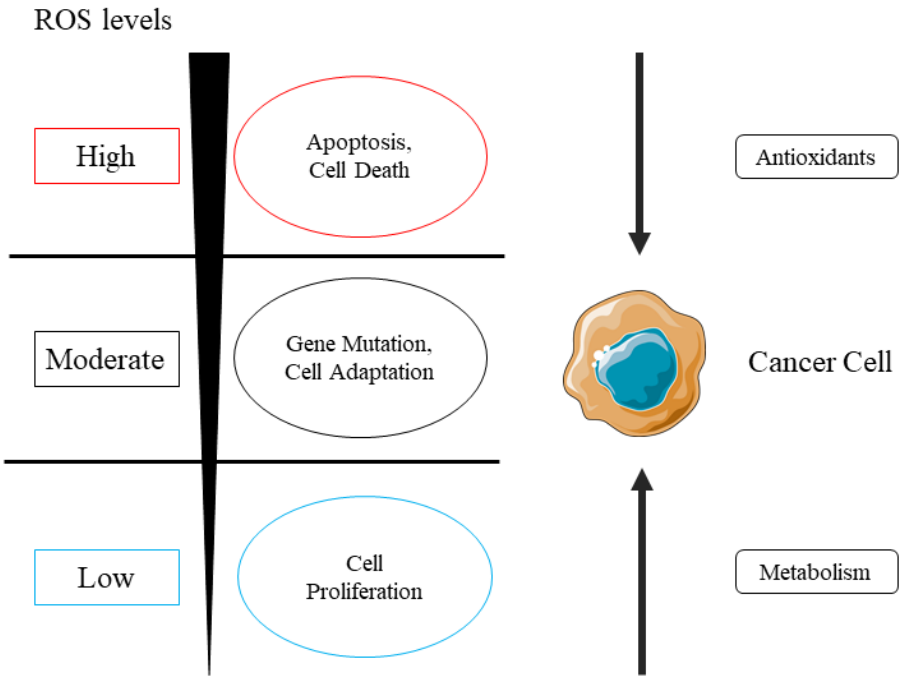

Figure 2: Relationship between the levels of ROS and cancer.

The effect of ROS on cell fate depends on the level of ROS present in cells. Low levels of ROS (blue) provide a beneficial effect, supporting cell proliferation. However, once ROS levels become too high (red), they can cause harmful oxidative stress, which can lead to apoptosis and cell death. To counteract this oxidative stress, cells use antioxidants to prevent ROS from accumulating at high levels. In a cancer cell, abnormal metabolism and protein translation produce abnormally high levels of ROS. through additional mutations and adaptations, the cancer cell tightly regulates ROS and antioxidants so that the cell survives, and the level of ROS is reduced to moderate levels (black). This accurate control of ROS levels enables cancer cells to avoid the deleterious effects of high levels of ROS, but also increase the chances that cells will experience additional ROS-mediated mutagenic events and stress responses that promote tumorigenesis.

1.4 Oncometabolites and their impact on cancer

Various studies have demonstrated that mitochondrial genes encoded by nuclear and mitochondrial DNA are mutated in cancer, a phenomenon associated with poor clinical outcome and prognosis (Gaude and Frezza, 2016). Even so, not all cancers can be discovered with mitochondrial dysfunction, and it should be emphasised that complete loss of mitochondrial function is detrimental to cancer cells (Gaude and Frezza, 2014). In recent years, the identification of cancer-associated mutations in genes that have an impact on cellular metabolism has attracted considerable attention (Ward and Thompson, 2012). Some of these mutations lead to the abnormal production of certain metabolites associated with cancer progression, called “oncometabolites”. Researchers have revealed the aberrant production of 2-hydroxyglutarate (2-HG), succinate and fumarate in cancer and linked them to cellular metabolic transformations and biological processes (Prasun et al., 2015; reviewed by Xiang *et al.*, 2020). Due to genetic and epigenetic alterations, reprogramming of cancer cell metabolism can affect the metabolic phenotype and anabolic production of cancer cells, accordingly enhancing the downstream oncogenic cascade (Kaelin Jr and McKnight, 2013) .

Succinate is a key metabolite of the tricarboxylic acid cycle (TCA) and plays an important role in cellular biological processes (Zhao et al., 2017). Succinate dehydrogenase (SDH) is an enzyme complex composed of four subunits (SDHA, SDHB, SDHC, SDHD), also known as mitochondrial complex II of the mitochondrial ETC (Yang et al., 2013a). Defects in SDHB, SDHC, and SDHD are associated with dysfunction of complex II in mitochondria (Wojtovich and Foster, 2014) and impaired the oxidation process of succinate to fumarate. Furthermore, loss-of-function mutations in SDH and concomitant

succinate overproduction have been associated with cancer development (Oermann et al., 2012). However, proper SDH function requires the involvement of oxidized FAD^+ and NAD^+ as cofactors, which are in insufficient supply in cancer cells because of mitochondrial dysfunction (Van Vranken et al., 2015). Succinate accumulation promotes angiogenesis by stimulating succinate receptor 1 (SUCNR1) and is accompanied by upregulated expression of vascular endothelial growth factor (VEGF) (reviewed by Xiang *et al.*, 2020). In addition, succinate accumulation activates pathways associated with epithelial-to-mesenchymal transition (EMT), tumor migration and invasion (Park et al., 2018). As expected, SDH deficiency was associated with metabolic reprogramming of cancer cells and promoted a glycolytic, pseudo-hypoxic phenotype. In hepatocellular carcinoma (HCC) cell lines, knockdown of SDHB resulted in reduced expression of ETC's complex III and IV and increased acidity in the cytoplasm, suggesting a shift from mitochondrial respiration to glycolysis as the primary energy source in cancer cells, the so-called Warburg effect (Tseng et al., 2018) (Figure 3).

Fumarate is an important candidate of the TCA cycle. Loss of function of fumarate hydratase (FH) is associated with overproduction of fumarate and causes hereditary leiomyomatosis and renal cell cancer (HLRCC) (Oermann *et al.*, 2012). High levels of fumarate can adjust the balance of biochemical reactions in which this oncometabolite acts as a substrate or product. For example, accumulation of fumarate has been shown to affect the conversion of succinate to fumarate in the TCA cycle, leading to disturbance in mitochondrial respiration associated with SDH (Johnson et al., 2018). Fumarate accumulation also caused a reprogramming of metabolism towards argininosuccinate-accumulation through the reversal of the urea cycle (Schmidt et al., 2020). Notably, cells with FH mutations require a continuous supply of exogenous arginine to keep the urea cycle active and the system is down when arginine supply is insufficient, creating a cancer-specific vulnerability. Similarly, fumarate accumulation promotes adenylosuccinate overproduction by reversing adenylosuccinate lyase (ADSL) in the purine nucleotide cycle (PNC) (Schmidt *et al.*, 2020). In contrast to succinate, fumarate also alters the post-translational modification of cysteine residues of several proteins, called succination. Succination induction by FH deficiency leads to inhibition of mitochondrial respiration, activating antioxidant responses as well as tumor growth (Johnson *et al.*, 2018; Yang et al., 2013b). In addition, FH-deficient cells reprogram their

metabolism toward aerobic glycolysis to provide energy (King et al., 2006). As a result, part of the carbon from glucose is transferred to the pentose phosphate pathway (PPP) to maintain redox homeostasis (Yang *et al.*, 2013b).

Accumulation of the 2-HG enantiomers L-2HG or D-2HG can be found in the following conditions: a) as pathological metabolites produced by lactate dehydrogenase (LDH) or malate dehydrogenase (MDH), respectively, in hypoxic cancer cells (Intlekofer et al., 2015); or b) as a result of gain-of-function mutations in the genes encoding isocitrate dehydrogenase 1 or 2 (IDH1 or IDH2) (reviewed by Xiang *et al.*, 2020). Thereby, LDH and MDH appear to be the main enzymes responsible for the production of L-2HG in the circumstances of hypoxia (Intlekofer *et al.*, 2015; Intlekofer et al., 2017), and overproduction of D-2HG is associated with gain-of-function mutations in IDH (Intlekofer *et al.*, 2017). In addition, accumulation of L-2HG has also been observed in renal cell carcinomas as well as in children with defective ETC components, respectively (Mullen et al., 2014). Interestingly, the aforementioned 2-HG, succinate and fumarate act as competitive inhibitors of α-ketoglutarate (αKG)-dependent dioxygenases (αKGDD) (Kolukula et al., 2014). The family of αKGDDs uses O_2 and αKG as cofactors for a range of oxidative reactions, such as chromatin modification or regulation of protein stability, such as hypoxia-inducible factors (reviewed by Xiang *et al.*, 2020). Various epigenetic enzymes belong to the family of α-KG-dependent enzymes, such as α-KG-dependent histone lysine demethylases (KDMs) and ten-eleven translocator (TET) DNA demethylases, with documented regulatory functions in DSB repair (Sulkowski et al., 2017).

The oncometabolites mentioned above would impair DNA repair process by inhibiting KDMs and TET DNA demethylases thus leading to histone/DNA hypermethylation, (reviewed by Xiang *et al.*, 2020). The effect on DNA repair of oncometabolites, dependent on the regulation of αKG-dependent epigenetic enzymes, offers new and exciting routes for cancer cell specific radiosensitization and meliorates RT denouement. (Figure 3)

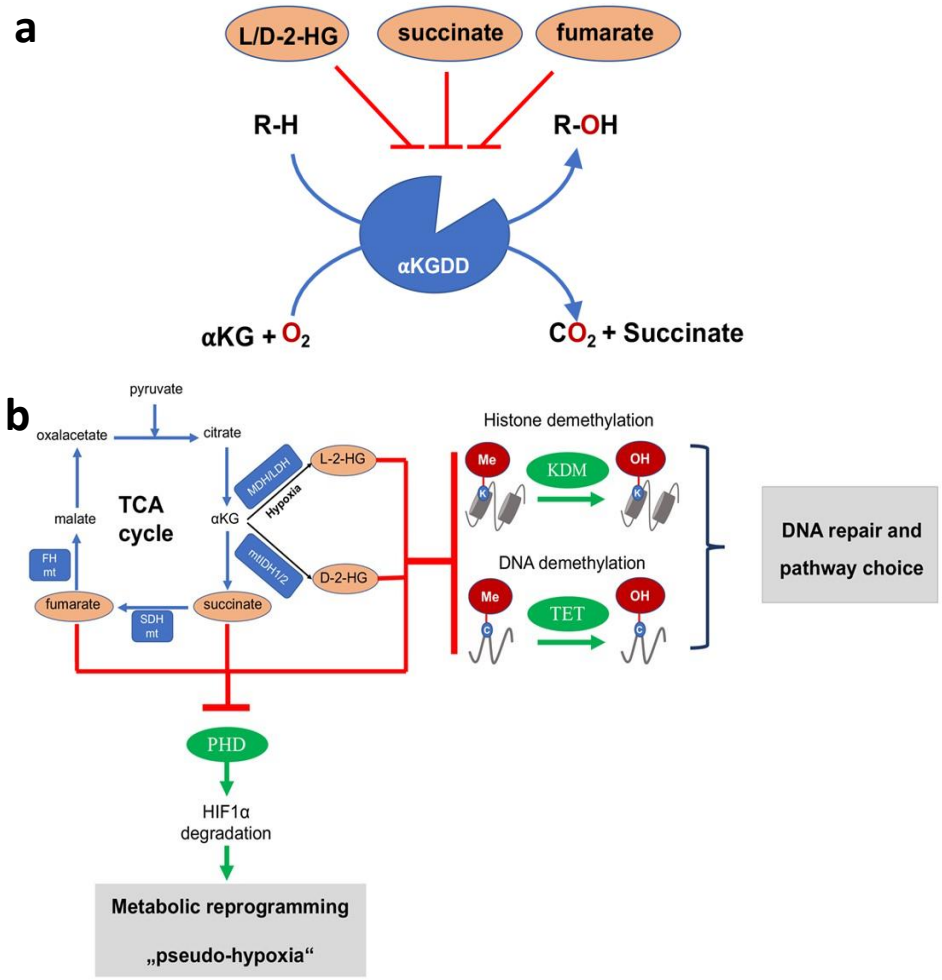

Figure 3: 2-HG, succinate and fumarate are antagonists to αKG and broadly inhibit αKG-dependent dioxygenases (αKGDDs).

a) αKGDDs use O_2 and αKG as co-factors to perform a range of oxidation reactions gaining succinate, CO_2 and hydroxylated target molecule. **b)** The indicated oncometabolites can accumulate as a consequence of mutations of TCA cycle enzymes or environmental cues, such as hypoxia and even without oncogenic mutations. 2HG, succinate and fumarate are competitive inhibitors of aKGDDs, thereby affecting DNA repair and pathway choice and offer novel therapeutic opportunities with IR. αKG=a-Ketoglutarate, L/D-2-HG= L/D-2-hydroxyglutarate, R=target molecule, K=Lysin, C=cytosine. (reviewed by Xiang *et al.*, 2020).

1.5 Mitochondrial citrate carrier

Mitochondria are labelled as sealed membrane structure which can be divided into inner membrane and outer membrane. Mitochondrial outer membrane separates the

mitochondrial from cytoplasm of the cell (Sherratt, 1991). However, the communication between mitochondria and other parts of the cell can be conducted by a large number of integral membrane proteins called porins. Porins are the major components which build channels on the mitochondrial outer membrane to transport relatively low molecular weight materials (such as ATP, NAD) between the intermembrane space and cytoplasm (Frey and Mannella, 2000; Sakaue and Endo, 2019). Mitochondrial inner membrane constitutes cristae through infolding into the inner space of mitochondrial in the purpose of providing bountiful platform for reactions including: a) Energy metabolism (such as ETC redox reactions), b) ATP synthesis, c) metabolite and nucleotide transportation into and out of the mitochondrial matrix (Frey and Mannella, 2000).

Mitochondrial carrier family (MCF) or the solute carrier family 25 (SLC25 protein family) is composed of a superfamily of membrane transporters which provide entity for biomolecules shipping. In humans, the MCF is made up of 52 members encoded by nuclear genes (Perland and Fredriksson, 2017). Members of the SLC25 family of transporters, which constitute the largest group of solute carriers, are also known as mitochondrial carriers (MCs). Compared with normal cells, the mitochondria displays increased transmembrane potential in cancer cells (Perland and Fredriksson, 2017). SLC25 family members can be classified into the following groups: carriers for amino acids (e.g. aspartate, glutamate (AGC)), nucleotides (e.g. ADP and ATP (AAC)), carboxylates (e.g. dicarboxylates (DIC), citrate (CIC)), inorganic ions (e.g. phosphate (PIC), sulphate (UCPs)), and other substrates (Ruprecht and Kunji, 2020).

The mitochondrial citrate transporter gene, SLC25A1 or CIC, maps on chromosome 22q11.21, a region amplified in some tumors (Catalina-Rodriguez et al., 2012). The main function of CIC is promoting the outflow of citrate across the mitochondria and import malate in, adjusting the relative concentration of pivotal TCA metabolites (Figure 4). In cancer cells, CIC upholds the basis of mitochondrial integrity and energy metabolism, avoiding mitochondrial damage or depletion via autophagy, to stimulate abnormal proliferation. Citrate mainly comes from TCA cycle via glucose-derived pyruvate, it can be oxidized in TCA cycle and OXPHOS in mitochondria and supports lipid synthesis in cytoplasm (Icard et al., 2012). As for malate, which maintains the proper function of TCA cycle, is correlated with proton importing when exchanging with citrate (Owen et al., 2002). On the basis of accelerated metabolic change in tumor cells, it has been proposed

that citrate is prevalently exported out of the mitochondria to provide ingredient which can be utilized for lipid, acetyl-Coenzyme A and macromolecular synthesis (Mullen *et al.*, 2011). It has been demonstrated that CIC promotes tumorigenesis, while its inhibition could suppress tumor growth (Catalina-Rodriguez *et al.*, 2012). Beyond that, CIC inhibition rewires the lipogenic program through attenuating the signal from peroxisome proliferator-activated receptor gamma, an important regulator of glucose and lipid metabolism, thus suppress the expression of gluconeogenic genes (Tan et al., 2020).

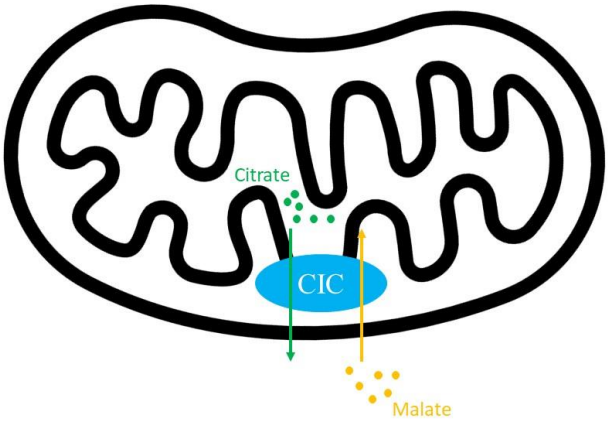

Figure 4: The mitochondrial citrate transporter (CIC) locates within the inner membrane of mitochondria.

CIC provides the connection between the mitochondrial matrix and cytoplasm by transporting citrate out of mitochondria in exchange for malate from cytoplasm.

1.6 Previous work and aims of the present thesis

Previous work in my group has demonstrated a role of the mitochondrial carrier proteins, particularly the citrate transport protein (SLC25A1) and the mitochondrial dicarbocylate carrier protein (SLC25A10) in cancer cell radiosensitivity in the context of acute and chronic cycling severe hypoxia with intermittent reoxygenation (Hlouschek *et al.*, 2018a; Hlouschek *et al.*, 2018b).

In more detail, previous MD student observed that adaptation of cancer cells to repeating cycles of anoxia and reoxygenation increased SLC25A1 expression in cancer cells *in vitro*.

Moreover, analysis of publicly available databases revealed that SLC25A1 overexpression was associated with reduced overall survival in lung, breast and head & neck cancer patients, particularly upon surgery with tumor-free margins in lung cancer patients. High SLC25A1-expression supported increased antioxidant defence of anoxia/reoxygenation-tolerant cancer cells thereby increasing their ability to cope with the oxidative damage induced by exposure to IR (Hlouschek *et al.*, 2018a). Of note, inhibition of SLC25A1 not only affected cellular and mitochondrial redox homeostasis but also increased the accumulation of the pathologic metabolite 2HG. Increased accumulation of 2HG was associated with slowed repair of radiation-induced DNA damage in these cells, and thus impairment of a critical determinant of radiation resistance (Hlouschek *et al.*, 2018a). These findings corroborated the importance of SLC25A1 in human pathologies observed by others for cancer and cancer radiosensitivity and make SLC25A1 a promising therapeutic target for tumor cell-specific radiosensitization in patients with high SLC25A1 expression (Hlouschek *et al.*, 2018a; Hlouschek *et al.*, 2018b; Prasun *et al.*, 2015).

Taken together, our previous work revealed that pharmacologic inhibition of SLC25A1 interferes with redox homeostasis and energy metabolism and also affects DNA repair, presumably by inducing accumulation of 2HG. Preliminary work further suggests that interference with SLC25A1 may induce a defect in DSB-repair by HRR (HR-ness) a thus be suited to sensitize cancer cells to clinically relevant DNA repair inhibitors *in vitro* (Kalthoff C, unpublished data). However, despite the pathologic roles of SLC25A1, the mechanisms connecting SLC25A1 inhibition and accumulation of 2HG are not fully understood. Moreover, the functional consequences of 2HG accumulation in response to SLC25A1-inhibition for the repair of radiation-induced DNA damage remained unclear. Finally, there may be further metabolic bottlenecks that are able to increase 2HG levels and may thus be suited to increase the cytotoxic action of RT.

Therefore, the aims of the present thesis were to further explore mechanisms underlying pharmacologic induction of HR-ness by metabolic inhibition, and their use for cancer cell-specific radiosensitization. Specifically, I focused i) on metabolic pathways and drugs inducing the accumulation of 2HG, ii) the mechanisms underlying 2HG-induced radiosensitization, and iii) the use of 2HG-inducing treatments for improving RT outcome in combination with DNA-repair inhibitors *in vivo*.

2 Materials and Methods

2.1 Materials

2.1.1 Chemical reagents and Buffers

Acetic acid	Sigma-Aldrich, St. Louis, USA
Coomassie Brilliant Blue	Carl Roth, Karlsruhe, Deutschland
Crystal violet	Carl Roth, Karlsruhe, Germany
Dihydroethidium (DHE)	Sigma-Aldrich, St. Louis, USA
Dimethylsulfoxid (DMSO)	Sigma-Aldrich, St. Louis, USA
DTAB	Sigma-Aldrich, St. Louis, USA
Ethanol 100%	Carl Roth, Karlsruhe, Germany
Fluorescence Mounting Medium	Agilent, Santa Clara, USA
Formaldehyde 37%	Carl Roth, Karlsruhe, Germany
Glutaraldehyde (1%)	Carl Roth, Karlsruhe, Germany
Glycerol	Carl Roth, Karlsruhe, Germany
Glycin	MERCK, Darmstadt, Germany
Hoechst 33342	Thermo Fisher, Waltham, USA
HCl	Carl Roth, Karlsruhe, Germany
Isopropanol	Sigma-Aldrich, St. Louis, USA
Methanol	Carl Roth, Karlsruhe, Germany
MitoSOX Red Mitochondrial Superoxide Indicator	Thermo Fisher, Waltham, USA
Normal goat serum (NGS)	Gibco, Gaithersburg, USA
Na_2EDTA	Carl Roth, Karlsruhe, Germany
NaOH	Carl Roth, Karlsruhe, Germany
NaCl	Carl Roth, Karlsruhe, Germany
Paraformaldehyde (PFA)	MERCK, Darmstadt, Germany
Phosphate buffered solution (PBS)	Gibco Life Technologies
Propidium iodide (PI)	Carl Roth, Karlsruhe, Germany
Sodium citrate	MERCK, Darmstadt, Germany
sodium lauryl sarcosinate	Sigma-Aldrich, St. Louis, USA
Triton X-100	MERCK, Darmstadt, Germany
Trizma® base	Sigma-Aldrich, St. Louis, USA

2.1.2 Cell culture

CASYton	Omni Life Science, Bremen, Germany
Dulbecco's Modified Eagle Medium (DMEM)	Gibco, Gaithersburg, USA
Fetal calf serum (FCS)	Biochrom, Berlin, Germany
Penicillin/Streptomycin (P/S)	Sigma-Aldrich, St. Louis, USA
Phosphate buffered solution (PBS)	Gibco, Gaithersburg, USA
RPMI1640	Gibco, Gaithersburg, USA
Trypsin (0,05% EDTA)	Biochrom, Berlin, Germany

2.1.3 Devices

AxioObserver.Z1 Fluorescence Microscope (with Apotome)	Zeiss, Oberkochen, Germany
Biological irradiator X-RAD 320 Precision X-Ray	North Branford, USA
CASY Cell Counter & Analyzer	Omni Life Science, Bremen, Germany
Colony Counter GelCount	Oxford Optronix, Oxford, UK
Electrophoresis power supply	VWR, Darmstadt, Germany
ELISA Reader	Synergy HT Bio-Tek
Flow Cytometer FACS Calibur	BD Bioscience, Franklin Lakes, USA
CytoFLEX Flow Cytometer	Beckman Coulter, Indianapolis,USA
Colony Counter GelCount	Oxford Optronix, Oxford, UK
Incubator C200	Labotect,Göttingen, Germany
Laminar flow bench	BDK, Sonnenbühl-Genkingen, Germany
Microplate Reader Synergy HT	BioTek, Winooski, USA
Microscope DM IRB	Leica Microsystems, Wetzlar, Germany
Microtiter Shaker MTS 2/4	IKA, Staufen, Germany

Multichannel pipette	Eppendorf, Hamburg, Germany
Pipettes (10 µL, 20 µL, 100 µL, 200 µL, 1000 µL)	Gilson, Middleton, USA
Pipetting aid	Hirschmann, Eberstadt, Germany
Thermomixer comfort	Eppendorf, Hamburg, Germany
Vortex Mixer Vortex-Genie 2	Scientific Industries, Bohemia, USA
Centrifuge 5417R	Eppendorf, Hamburg, Germany
Centrifuge CR 4.22	Jouan SA, Saint-herblain, France
Centrifuge Z216M	Hermle, Wehingen, Germany
Seahorse XFe96 Analyser	Agilent, Santa Clara, USA

2.1.4 Solutions

2.1.4.1 FACS

DHE-Solution	5 µM in PBS
MitoSOX	5 µM in medium
Nicoletti-Solution	0,1 % Sodium citrate 0,1 % TritonX 100 50 µg/ml Propidium iodide
PI-Exclusion-solution	5 µg/ml PI in PBS
FACS Flow	BD Biosciences
FACS Clean	BD Biosciences
FACS Rinse	BD Biosciences
Foxp3 / Transcription Factor Staining Buffer Set Fixation/Permeabilization Concentrate Fixation/Permeabilization Diluent Permeabilization buffer 10X	eBioscience
FACS buffer	2500ul FCS (0.5%) 2000ul EDTA (0.5M)

	500 ml PBS

2.1.4.2 Alkaline CometAssay

Agarose NEEO ultra-quality	Carl Roth
Lysis Solution A1(pH>13)	1.2M NaCl 100mM Na2EDTA 0.1% sodium lauryl sarcosinate 0.26M NaOH
Electrophoresis solution A2(pH 12.3)	0.03M NaOH 2mM Na2EDTA

2.1.4.3 Colony formation assay

3.7% formaldehyde	
70% ethanol	
Coomassie Brilliant Blue staining solution (0.05%)	20% methanol 7.5% acetic acid 0.05% Coomassie Blue

2.1.4.4 NAD/NADH and NADP/NADPH assay

Base solution with 1% DTAB	0.2M NaOH 1% DTAB
HCl/Trizma® solution	0.4M HCl 0.5M Trizma® base

2.1.4.5 Mitochondrial function

Seahorse XF Media	Agilent
Seahorse XF Calibrant	Agilent
Sodium pyruvate	Sigma-Aldrich
L-glutamine	Gibco
Glucose	Carl Roth

2.1.5 Kits

D2HG Assay Kit	Biovision, Zurich, Switzerland
NAD/NADH-Glo Kit	Promega, Madison, Wisconsin, USA
NADP/NADPH-Glo Kit	Promega, Madison, Wisconsin, USA
GSH/GSSG-Glo Kit	Promega, Madison, Wisconsin, USA
Seahorse XF Cell Mito Stress Test Kit	Agilent, Santa Clara, USA

2.1.6 Treatments

2-((4-chloro-3-nitrophenyl) sulfonamido) benzoic acid (CTPI2)	MedChemExpress, New Jersey,USA
PJ34 hydrochloride (PARPi)	abcam, Cambridge, UK
a-ketoglutarate	Sigma-Aldrich, St. Louis, USA
Octyl-D-2HG	Sigma-Aldrich, St. Louis, USA
Nicotinamide (NAM)	Sigma-Aldrich, St. Louis, USA
JIB-04	Sigma-Aldrich, St. Louis, USA

2.1.7 Consumables

1.5 mL Microcentrifuge tubes	Sarstedt, Nümbrecht, Germany
2 mL Microcentrifuge tubes	Sarstedt, Nümbrecht, Germany
CASYcups	Omni Life Science, Bremen, Germany
CELLSTAR Seroglogical Pipette(5 mL, 10 mL, 25 ml)	Greiner Bio-One, Kremsmünster, Austria
FACS tube	Greiner Bio-One, Kremsmünster, Austria
Falcon tube (15 mL, 50 mL)	Greiner Bio-One, Kremsmünster, Austria
Slide	Engelbrecht, Edermünde, Germany
Pipette tips (10 µL, 100 µL/200 µL, 1000 µL)	STARLAB, Hamburg, Germany
Cell culture flasks (T25/T75/T175)	Greiner Bio-One, Kremsmünster, Austria
6-well tissue culture plate	Eppendorf, Hamburg, Germany
12-well tissue culture plate	Sigma-Aldrich, St. Louis, USA
96-well cell culture plate	Sigma-Aldrich, St. Louis, USA
Seahorse XF Cell Culture Microplate	Agilent, Santa Clara, USA

Seahorse XF sensor cartridge	Agilent, Santa Clara, USA

2.1.8 Antibody

γH2AX (Alexa Fluor 647)	BD Pharmingen	Ratio: 1:100

2.1.9 Cell lines

A549	Non-small cell lung cancer (NSCLC)
U87MG	Glioblastoma
NCI-H460	NSCLC
T98G	Glioblastoma

2.1.10 Software

Axio Vision LE64	Carl Zeiss
Cytometrische Analyse software FlowJo	FloJo Enterprise
Gel Count	Oxford Optronix
ImageJ	Wayne Rasband
Imaris - Microscopy Image Analysis Software	Oxford Instruments
Wave	Agilent
GraphPad Prism 7.0	GraphPad Software

2.2 Methods

2.2.1 Cell culture

2.2.1.1 Cultivation of cells

Seeding, cultivation and most of the pre-treatments of the different cell lines, were performed under sterile conditions at suitable workstations. Each cell line received the optimal medium (see Table 1.1). Any material used was either autoclaved before and after use or was disposable and discarded after use. In accordance with the cell growth, these were regularly split, and the medium was renewed in order to obtain optimal conditions in terms of cell number and cell density for the experimental projects.

Table 1: Media used for the cell lines

Cell lines	Medium
A549	DMEM +10% FCS+1.5% Pen/Strep
NCI-H460	DMEM +10% FCS+1.5% Pen/Strep
T98G	DMEM +10% FCS+1.5% Pen/Strep
U87MG	DMEM +10% FCS+1.5% Pen/Strep

2.2.1.2 Splitting and medium change

In order to maintain cell density and cell number in the optimal range, the cells had to receive new medium on a regular basis. For this purpose, the medium was aspirated from bottles in which the cells adhered to the bottom using a sterile pipette, and the cells were then washed once with PBS. The PBS was also removed afterwards. New medium was added according to the bottle size. As soon as the flasks exceeded an optimal cell density or more cells were needed, they will be split. The medium was removed, and the cells were washed once with PBS. The cells were then incubated with 5x TE for a short time to detach them from the bottom of the flask. The reaction was stopped with medium and transferred to new flasks at a ratio of 1:10 or 1:20 as required. There they again received new medium according to the ratio. Cells were incubated under standard cell culture conditions (37 °C, 21 % O_2, 5 % CO_2).

2.2.1.3 Preservation of cells

To preserve cells for later use, a nitrogen tank was utilized to freeze them. For this purpose, the cells were first pre-treated with trypsin as described in 2.2.1.2 to detach them from the bottom of the culture flask or dish before adding medium to stop the trypsinization. After collection of the cell suspension was finally pelleted for 4 min at 1500 rpm and this pellet was again resuspended in DMEM + 10% FCS + 10% DMSO. This suspension was transferred to cryogenic vessels and first stored overnight in an isopropanol freezing vessel at -80 °C to cool slowly and to avoid damage to cells. One day later the cryogenic vessels were put into liquid nitrogen.

2.2.1.4 Thawing of cells

To thaw the previously preserved cells, they were first thawed in a 37°C water bath. The cell suspension was then taken up in DMEM + 20% FCS + 1.5% Pen/Strep and transferred to flasks. After 24h, medium was changed to DMEM + 10% FCS + 1.5% Pen/Strep.

2.2.1.5 Treatment of cells

2.2.1.5.1 Cell counting

To ensure comparability of the experiments, the same cell numbers were required. To determine these, CASY Cell Counter was at our disposal. In order to use it, a cell suspension was generated from the cultured flasks by trypsinization and washing with PBS. From this suspension, a 1:200 dilution with CASY ton was generated in specially provided CASY cups. This was placed in the CASY Cell Counter in such a way that a fine capillary reached into the suspension, through which the device draws in liquid via a vacuum. In this capillary, the resistance generated by the cell chain is measured. This correlates directly with the number of cells with an intact cell membrane (vital cells). By measuring the number of cells in the 1:200 dilution, the amount of suspension needed for plating could be calculated.

2.2.1.5.2 Drug treatment

Depending on the experiment, cells were pretreated between 2 hours before irradiation. The following agents were used for treatment:

Table 2: Active ingredients for treatment

Drug name	Manufacturer	Solvent	Concentration
CTPI2	MedChemExpress	DMSO	200µM
a-ketoglutarate	Sigma-Aldrich	H_2O	8mM
octyl-D-2HG	Sigma-Aldrich	DMSO	150µM
Nicotinamide (NAM)	Sigma-Aldrich	H_2O	1mM
PARP inhibitor (PJ34)	Calbiochem	DMSO	4µM

After treatment, cells were incubated again until each experiment. Untreated cells or cells treated with the drug solvent from the same passage served as controls.

2.2.1.5.3 Irradiation of the cells

For IR, an X-RAD 320 beam machine at 320 kV, 12.5 mA and a 1.65 mm aluminium filter were applied at room temperature to carry out photon radiation. The distance to the cells was 50cm. The total dose of 0-30 Gy depended on the experiment and was produced at a rate of 3.7 Gy/min. Control cells were sham irradiated at room temperature for the same period of time as their irradiated counterparts. After irradiation, the cells were incubated again at 37°C and 5% CO_2.

2.2.2 Crystal violet assay

The crystal violet assay was used to quantify cell viability by measuring the amount of nuclear DNA of viable adherent cells.

For this purpose, cells were plated in 96-well plates. The number of cells was 7500 cells/well. After 24h incubation, these cells were treated with different concentrations of treatment and irradiated with 0 or 5Gy photons after another 2h incubation. The cells were stained with crystal violet 24h or 48h after treatment. To discard dead cells or cells that did not adhere, the medium was discarded, and the 96-well plates were carefully washed

with PBS. Cells were then fixed using glutaraldehyde (1% in PBS) for 15min. The solution was removed and crystal violet stain was added to the cells for 25min instead. After removal of the dye, the cells were carefully washed again, now with distilled water, and the cells were then permeabilized on a shaker using Triton X-100 (0.2% in PBS) for half an hour. This ensured the release of the dye from the vital cells. The absorbance could then be determined with an ELISA reader using a wavelength of 540nm. The absorbance measured is directly proportional to the number of vital cells.

2.2.3 Flow cytometry

Flow cytometry allows the analysis of up to one thousand cells per second with respect to size, fluorescence and granularity. After the necessary preparation, cells are sucked through a measuring capillary by means of overpressure. A stream of cells is generated which is directed past a laser beam and deflects it in a manner specific to various properties. The scattered light is then detected by photodetectors. The scattering is divided into forward scattered light (FSC) and side scattered light (SSC), where the former can be used to measure the relative cell size and the latter for cell granularity. In turn, fluorescence intensities can be derived from the different wavelengths. This intensity is analyzed by the absorption and re-emission of the light emitted by the laser by the fluorochrome. This emission light is now directed to optical detectors. The number of fluorochrome molecules detected is proportional to the emitted fluorescence light and is displayed in a diagram or histogram. In a histogram, a frequency distribution of the fluorescence signals can also be seen afterwards.

However, before the cells are measured and analyzed by the flow cytometry instrument, they must first be prepared. For this purpose, 300,000 cells for each sample are plated in a 6cm Petri dish and then incubated for 24h. The cells are now pretreated or not pretreated according to the experiment, 2h before the planned irradiation. This is again done by photon beam with the doses 0 or 5 Gy. Thereafter, the cells were again incubated for 6, 24, 48 or 72h for different purpose. For staining the cells, the medium was first removed from the plates and transferred to FACS tubes. The plates are now washed 1x with PBS and the PBS is also added to the tubes. The cells are then treated with trypsin and incubated at 37°C for 3-5 min to detach from the plates. By resuspending with the

previously removed medium, the reaction of the trypsin is stopped and the remaining cells are also detached. Now the whole suspension is divided among the FACS tubes, according to the planned stainings. In our case, each sample was divided into 4 tubes for subsequent ROS-staining with DHE, mitochondrial ROS staining with MitoSOX, determination of fragmented DNA by propidium iodide (PI)-staining in a hypertonic buffer (Nicoletti, 51) and cell death by exclusion PI (ExPI)-staining. The tubes are centrifuged at 1500 rpm for 6 min to obtain a cell pellet. Carefully discard the supernatant and resuspend the pellet with 200 µl of the prepared stains and vortex. The Nicoletti and ExPI stains were incubated for 30min at room temperature in the dark, and the DHE and MitoSOX stain were also incubated for 30min in the dark but in an incubator at 37°C.

2.2.3.1 Determination of cytoplasmic ROS levels

Staining of cell pellets with DHE (Dihydroethidium) is used to determine the levels of cytoplasmic ROS. When DHE is oxidized by ROS, ethidium is formed which intercalates into DNA. This intercalation shifts the previously blue fluorescence emitter to the green to red wavelength range (Wang and Zou, 2018). However, if DHE is not oxidized, it cannot penetrate into cells or intercalate into DNA. Thus, it is very suitable as a redox indicator for measuring oxidative processes in living cells.

2.2.3.2 Staining of mitochondrial ROS

MitoSOX reagent permeates live cells where it selectively targets mitochondria. It is rapidly oxidized by superoxide but not by other ROS and reactive nitrogen species (RNS). The oxidized product is highly fluorescent upon binding to nucleic acid (Kauffman et al., 2016).

2.2.3.3 Determination of apoptotic cells

With the help of a staining procedure developed by Nicoletti and colleagues (Nicoletti et al., 1991) it is possible to perform a cell cycle analysis in which the percentage of apoptotic cells is determined. By adding Triton X-100 to the hypotonic buffer, not only the cell membranes of apoptotic cells but also the membranes of healthy cells are

permeabilized so that the dye propidium iodide (PI) can be taken up. This serves to visualize the cell cycle of all cells. The proportion of apoptotic cells is visible in the diagram by the so-called sub-G1. This is caused by the fragmentation of DNA in these damaged cells by enzymatic digestion.

2.2.3.4 Determination of dead cells

Staining with propidium iodide (PI) also takes advantage of the different states of the cell membrane of living and dead cells. PI cannot cross an intact cell membrane and thus cannot enter living cells ("PI-exclusion"). However, this is possible in dead cells due to the permeable membrane. Due to intercalation into the DNA, the number of PI-positive cells increases and can be measured by FACS instrument.

2.2.3.5 Determination of DNA repair foci

Staining of γH2AX-foci is a method frequently used to determine the induction of DSB because the number of γH2AX-foci has been found to be proportional to the number of DSBs produced.

Cells were trypsinized with 1x TE for 5 min after washing with PBS, then stopped trypsinization with full medium, transferred detached cells from one well to Eppendorf tubes. Centrifuged tubes with cells at the condition of 4°C ,1500rpm for 5min, and then discarded supernatant from tubes. Resuspended the pellet with PBS to wash the cells and transferred them into new Eppendorf tubes. Centrifuged tubes with cells at the condition of 4°C ,1500rpm for 5min, and then discarded supernatant from tubes. Added 100µL Fix-Perm-Solution, which was consist of Fixation/Permeabilization Concentrate and Fixation/Permeabilization Diluent at the ratio of 1:4, to the cell-pellet and incubated at 4°C in the dark for 1h. Add 100µl Perm-buffer, which was the product of Permeabilization buffer 10X diluted in H2O at 1:10 ratio. Centrifuged for 6min at 1500 rpm at 4°C and discarded supernatant. 100µl staining solution (γH2A.X antibody 1:100 in Perm-Buffer) was used to resuspend the pellets before 30 minutes incubation at room temperature in dark. After that, 100µl Perm-buffer was added into tubes before centrifuging for 6min at 1500 rpm at 4°C and supernatant discarding. Finally, 100µl

FACS-Buffer was added to resuspend the cells before transferring into 5ml FACS tube for measurement. The result is demonstrated as γH2AX score, and formula for calculation is as follows:

γH2AX score = % γH2AX positive cells * fluorescence intensity of γH2AX positive cells

2.2.4 Colony formation assay (CFA)

To compare the long-term survival of cells under different conditions, such as non-treatment, irradiation, pharmacological treatment or combination therapy, I used the colony formation assay. In this assay, different numbers of cells per well were selected, which were in accordance with different radiation doses or different pharmacological treatments. From the resulting values, survival fractions of the individual treatment options can be calculated, thus illustrating the effectiveness of the respective strategy.

2.2.5 Alkaline Comet Assay

The alkaline comet assay is capable of detecting DNA double-strand breaks, single-strand breaks, alkali-labile sites, DNA-DNA/DNA-protein cross-linking, and incomplete excision repair sites (Pu et al., 2015). Gently detached cells from 6-well plate surface. Performing cell count and dilute 30.000 cells in 200 µl Agarose. 200 µl of the cell/Agarose was mixed onto the slide and cover with a coverslip immediately. Slides were put into 4°C in the dark (e.g. place in refrigerator) for 5 min and then gently removed the coverslip. Immersing slides in 4°C Lysis Solution A1 for 60 min or overnight. Draining excess buffer from slides and they were immersed in freshly prepared Alkaline electrophoresis solution A2 for 10 min. Putting slides in the electrophoresis chamber and run the electrophoresis for 1h at 20V (approx. 30mA set the upper limit to 500mA). Time and voltage should be established before running real experiment. Gently draining excess electrophoresis solution, and then put into dH2O for several seconds. After that,70-100% ethanol was used to drain the water from the slides for several seconds. Samples were put placed at RT until the surface is completely dry. 50µL of diluted propidium iodide was put onto each slide, and then put the coverslip on top and stain for 1-2 min (room temperature) in the dark. Slides were observed by fluorescence microscopy. At least 50

nuclei were taken photos for downstream analysis. ImageJ was used to analyse the nuclei photos.

2.2.6 D-2-Hydroxyglutarate measurement.

The Biovision colorimetric kit was used to measure D2HG levels. Cells were cultured in T175 flasks to obtain the required number of cells (1x10^7 cells) from each cell line for the assay. Pre-treatment with the respective drugs was done 6h before the start of the protocol. First, the cells were centrifuged and the supernatant was discarded. The cell pellet was resuspended with 100µl of ice-cooled D2HG buffer and incubated on an ice for 10 min. The sample was then centrifuged again at 10,000 rpm for 5 min at a temperature of 4°C. The supernatant was now transferred to new Eppendorf tubes. The experiment was plated in 96-well plates. For each cell line under investigation, 6 wells were needed, so that one had 3 untreated wells (ctrl) and 3 with treatment (e.g., CTPI2). In addition to the prepared samples, one needed the Reaction Mix, as well as the Background Control Mix, which one prepared anew for each experiment from the individual components of the kit.

Table 3: Preparation for the Mix reagent

	Reaction Mix	Background Control Mix
D2HG Assay Buffer	46 µl	48 µl
D2HG Enzyme	2 µl	0 µl
D2HG Substrate Mix	2 µl	2 µl

Reaction system:

Samples

- 2µl Sample
- 48µl Assay Buffer
- 50µl Reaction Mix

Internal Standard (Spiked)

- 2µl Sample
- 43µl Assay Buffer
- 5µl 1mM D2HG Standard

- 50µl Reaction Mix

External Standard

- 30µl Assay Buffer
- 20µl 1mM D2HG Standard
- 50µl l Reaction mix

Reagent Background

- 50µl Assay Buffer
- 50µl Background control mix

After pipetting together the different wells, the plate was placed on a shaker for 15 seconds and then incubated at 37°C for 1h. After that, the plates could be read using the ELISA reader at 450 nm. To calculate the D2HG concentrations from the measured values the following formula was used:

Figure 5: Formula to calculate the D2HG concentrations in the samples.

$$\text{D2HG amount (nmol)} = \left(\frac{(OD_{\text{sample (corrected)}})}{(OD_{\text{(spiked sample)}})\text{-}(OD_{\text{sample)}})}\right) * 5$$

2.2.7 NAD/NADH and NADP/NADPH assay

The NAD/NADH Assay is bioluminescent assay for detecting total oxidized and reduced nicotinamide adenine dinucleotides (NAD+ and NADH, respectively) and determining their ratio in biological samples. Similar to NAD/NADH Assay, NADP/NADPH Assay is designed for oxidized and reduced nicotinamide adenine dinucleotide phosphates (NADP+ and NADPH, respectively) and their ratio. Cells were plated in 96 well plate one day before treatment. 24h or 48h after treatment, supernatant of cells was removed and added 25µl PBS and 25µl of base solution with 1% DTAB to each well. Briefly mixing plate on a plate shaker to ensure homogeneity and cell lysis. Moving 25µl of each sample to an empty well for acid treatment. To these samples, adding 12,5µl of 0.4N HCl per well; these wells contained the acid-treated samples. The original sample wells are the base-treated samples. Covering the plate, incubated all samples for 15 minutes at 60°C. 10 minutes to equilibrate the plate and 12,5µl of 0.5M Trizma® base was added to each well of acid-treated cells to neutralize the acid. 25µl of HCl/Trizma® solution was

administered to each well containing base-treated samples. NAD/NADH and NADP/NADPH Detection Reagent were prepared according to table 1.4 and 1.5 before added to each well. Gently shaking the plate to mix before 60 minutes incubation at room temperature. Finally, luminescence was recorded using a luminometer.

Table 4: NAD/NADH Detection Reagent

Component	Volume for 1ml
Reconstituted Luciferin Detection Reagent	1ml
Reductase	5µl
Reductase Substrate	5µl
NAD Cycling Enzyme	5µl
NAD Cycling Substrate	**25**µl

Table 5: NADP/NADPH Detection Reagent

Component	Volume for 1ml
Reconstituted Luciferin Detection Reagent	1ml
Reductase	5µl
Reductase Substrate	5µl
NAD Cycling Enzyme	5µl
NAD Cycling Substrate	**5**µl

2.2.8 Mitochondrial function (Seahorse) measurement

The Agilent Seahorse XF Cell Mito Stress Test measures key parameters of mitochondrial function by directly measuring the oxygen consumption rate (OCR) of cells on the Seahorse XFe Extracellular Flux Analysers. Agilent Seahorse XFe Analyser must be warmed up one day before the assay. On the same day, 10.000 cells were seeded on the Seahorse XF Cell Culture Microplate and a sensor cartridge was hydrated in Seahorse XF Calibrant at 37 °C in a non-CO2 incubator overnight. On the assay day, assay medium was prepared by supplementing Seahorse XF DMEM medium with 1 mM pyruvate, 2 mM glutamine, and 10 mM glucose at first. Assay medium was added to Seahorse XF Cell Culture Microplate to replace the original one and the cell plate was put into 37 °C and non-CO2 incubator for 60 minutes. Compound stock solution and working solution preparation, as well as port loading strategy, were illustrated in table 1.6 and table 1.7. To start the assay, Wave software was applied and running procedure had been designed before running. Calibration plate with the loaded sensor cartridge was placed on the

instrument tray firstly. 15-30 minutes later, calibration plate was replaced with the cell plate. Hoechst luminescence reading was performed after the whole assay procedure to normalize cell number.

Table 6: Compound stock solution

Compound	Volume of assay medium	Stock concentration
Oligomycin	630 µL	100 µM
FCCP	720 µL	100 µM
Rot/AA	540 µL	50 µM

Table 7: Compound working solution

	Final well(µM)	Stock solution volume (µL)	Media volume (µL)	Volume added to port (µL)
Port A Oligomycin	1.0	300	2700	20
Port B FCCP	2.0	600	2400	22
Port C Rot/AA	0.5	300	2700	25
Port D Hoechst	200	200	3000	27

2.2.9 Chicken chorioallantoic membrane (CAM) assay

The chicken chorioallantoic membrane (CAM) is an experimental platform to study tumor genesis and growth in transplant biology, cancer research and drug development. Chicken eggs were incubated in the environment of relative air humidity of 65% and a temperature of 37°C with a static position for 10 days before grafting. On the grafting day, large vessel area was marked before opening the “window”. A hole was created at the bottom of the eggs with scissor, widen with tweezer. The chosen “window” was opened with drill. 2 million cells were resolved in 50 µL PBS which can be pipetted onto the chorioallantoic membrane of eggs. 7 days after grafting, the tumor was dissected and its diameters were measured.

2.2.10 Statistical evaluation

Statistical analysis was generated using GraphPad Prism 7.0, calculations of various formulas mostly using Microsoft Excel 2019. Experiments were repeated 3 times. Assuming a normal distribution, statistical significances were calculated. For this, I used

either the unpaired Students t-test or the two-way ANOVA (analysis of variance, means comparison test) with a post-hoc test according to Bonferroni. The confidence interval was 95%. The significance level was set at $\alpha = 0.05$ (equivalent to 5%), i.e., the difference between two data sets is significant if the p value $\leqslant 0.05$. Significances were marked with asterisks (*) in the Figures. Here, *p<0.05 stands for significant, **p<0.01 for highly significant, ***p<0.001 for extremely significant and ****p<0.0001 for most significant, ns for non-significant.

3 Results

3.1 Inhibition of SLC25A1 led to 2-HG production

In previous work of my group, the SLC25A1 inhibitor (SLC25A1i) 1,2,3-benzene-tricarboxylic acid (BTA) increased the levels of D-2-hydroxyglutarate (D-2HG) levels in oxic and anoxia-tolerant NCI-H460 cell lines (Hlouschek *et al.*, 2018a). Accordingly, the genetic inhibition of SLC25A1 in lung cancer (A549, NCI-H460) and glioblastoma (U87-MG, T98G) cell lines promoted D-2HG overproduction to a similar extend as BTA (MD-thesis of Christian Kalthoff; to be submitted). In the present thesis I used CTPI2, a novel small molecule inhibitor of SLC25A1 with increased specificity, to examine if this inhibitor will reproduce the effect of genetic SLC25A1 inhibition on D-2HG. As shown in Figure 6a, pharmacologic inhibition of SLC25A1 by application of CTPI2 for 6h induced significant increase in D-2HG levels of NCI-H460 cells line, thus reproducing the effects of a genetic downregulation by siRNA (MD-thesis of Christian Kalthoff; to be submitted). In addition, I performed time-resolved analyses of D-2HG modulation by CTPI2. The obtained data demonstrated sustained stimulation on D-2HG levels during 6 to 48h after CTPI2 treatment, hinting to a long-lasting D-2HG accumulation induced by SLC25A1 inhibition by CTPI2-treatment.

a

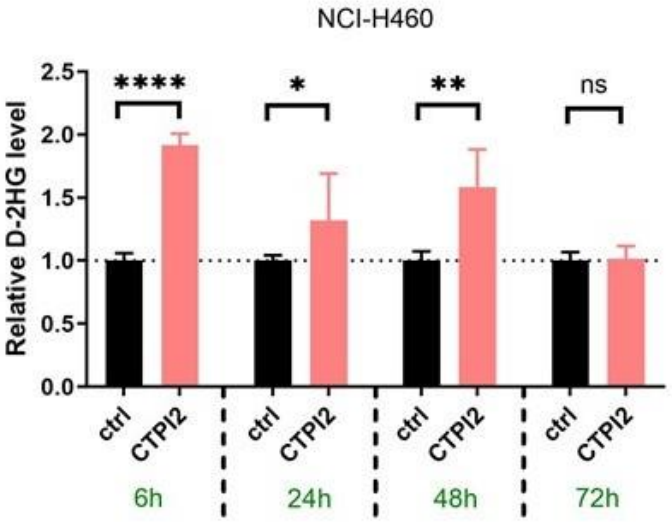
NCI-H460
Relative D-2HG level
2.5
2.0
1.5
1.0
0.5
0.0
****
*
**
ns
ctrl
CTPI2
6h
24h
48h
72h

b

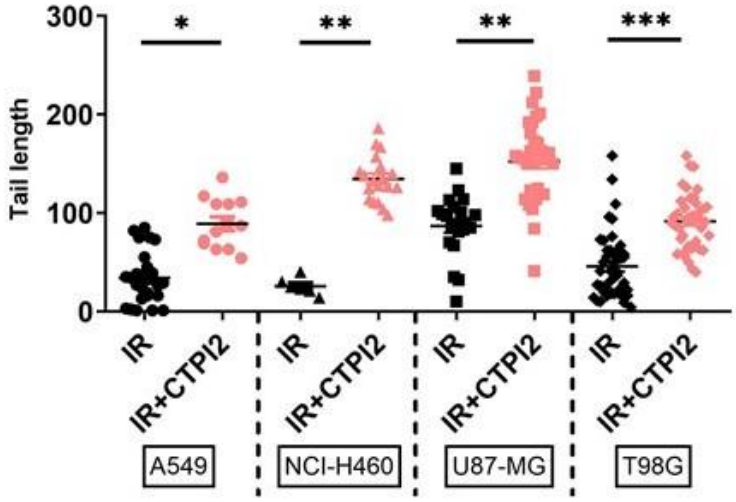
Tail length
300
200
100
0
*
**
**
***
IR
IR+CTPI2
A549
NCI-H460
U87-MG
T98G

c

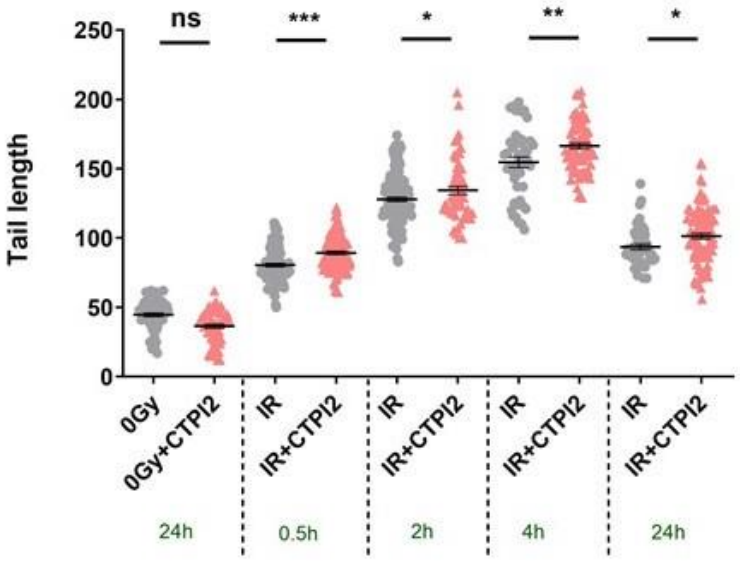
Tail length
250
200
150
100
50
0
ns
***
*
**
*
0Gy
0Gy+CTPI2
IR
IR+CTPI2
24h
0.5h
2h
4h
24h

Figure 6: Time dependent induction of D-2HG by SLC25A1 inhibition (CTPI2) and its relevance for radiation-induced DNA damage

A549, U87-MG, T98G and NCI-H460 cells were pre-treated for 2h with CTPI2 (200μM) alone and irradiated with a dose of 30Gy or left untreated as indicated. **a)** D-2HG production of 6-72h after CTPI2 (200μM) treatment alone in NCI-H460 cell line was investigated using the D-2HG assay kit. **b)** DNA damage induced by SLC25A1 inhibition (CTPI2) with IR (30Gy) in A549, NCI-H460, U87-MG and T98G cell lines were determined by alkaline comet assay 6h after treatment. **c)** Time dependent (0.5-24h) DNA damage induced by SLC25A1 inhibition (CTPI2) with IR (30Gy) as determined by alkaline comet assay in NCI-H460 cell line. Data represent the mean values (±SEM) from three independent experiments (N=3). Statistical significance: by non-parametric unpaired t-test. ns=not significant ($p > 0.05$), * $p < 0.05$, ** $p < 0.01$, *** $p < 0.001$, **** $p < 0.0001$.

3.2 CTPI2 or octyl-D2HG treatment potentiated radiation-induced DNA damage and radiosensitized NCI-H460 cells to IR

Next, I explored the hypothesis of metabolically induction of DNA-repair defects and associated radiosensitization by SLC25A1. Previous work by MD-Student Christian Kalthoff (to be submitted) revealed an accumulation of radiation-induced γ-H2AX foci in combination with CTPI2. In this thesis, I utilized the alkaline comet assay to quantify DNA damage induced by CTPI2 in combination with IR. As demonstrated in Figure 6b, treatment with CTPI2 increased DNA damage of A549, NCI-H460, U87-MG and T98G cell lines 6 h after IR-treatment compared to IR-treatment alone. What`s interesting, the alteration of balance between DNA damage and repair with time was revealed in this study. Here, CTPI2 treatment combined with IR significantly increased radiation-induced DNA damage within the first 4 h (Figure 6c) and elevated residual DNA damage 24h after treatment compared to IR-treatment alone, as demonstrated in NCI-H460 cancer cells.

In order to explore the mechanism behind the radiation-induced amplification of DNA-damage upon CTPI2 treatment, octyl-D-2HG, which is the cell membrane-permeable form of D-2HG, was introduced to the same cell line in order to dissect the direct effects of the oncometabolite D-2HG on radiation-induced DNA damage. DNA damage augmentation was also observed upon treatment with octyl-D-2HG application, although the effect of CTPI2 was more pronounced than that of the membrane-permeable D-2HG (Figure 7a-c).

Next, the ability of cells to repair radiation-indued DSBs upon CTPI2 treatment was explored by quantifying radiation-induced ɣ-H2AX foci using flow cytometry (Staaf et al., 2012). Compared with irradiated control, CTPI2 treatment resulted in higher numbers of γ-H2AX foci formation 6 h after IR, which implied that CTPI2 delayed the resolution of DSB repair foci in a specific manner. Here, the γ-H2AX foci readouts obtained by flow cytometry corroborated the γ-H2AX foci readouts collected by fluorescence microscopy method performed by Christian Kalthoff (MD-thesis to be submitted). In contrast to the determination of DNA damage by the alkaline Comet assay, octyl-D-2HG treatment had a more pronounced effect on the accumulation of γH2A.X foci compared to CTPI2-treatment (Figure 7d). Taking all the DNA damage process together, it could be concluded that CTPI2- and octyl-D2HG-treatment preserved radiation-induced DNA damage state at high levels, pointing to an inhibitory effect on DNA repair. The long-term effect of CTPI2 and octyl-D2HG treatment on the radiosensitivity of NCI-H460 cell line was investigated with colony formation assay (CFA). As demonstrated in figure 7e, both CTPI2 and octyl-D2HG treatment decreased the survival fraction (SF) of NCI-H460 cells in combination with IR-treatment. In Summary, CTPI2- or octyl-D2HG treatments increased radiation-induced DNA damage and thus radiosensitized NCI-H460 cells.

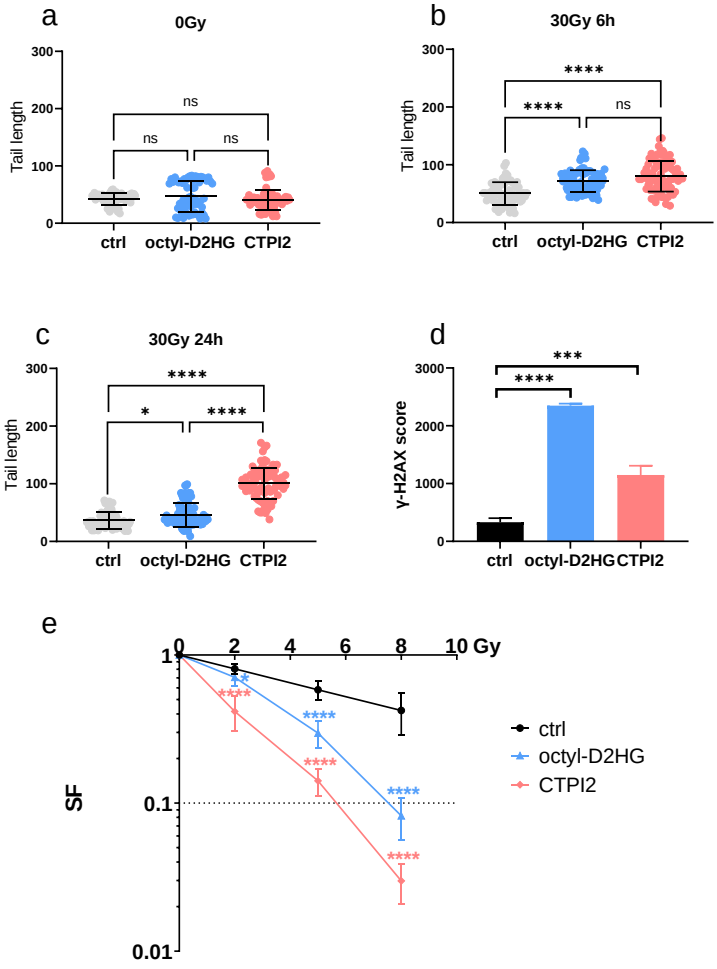

Figure 7: DNA damage induced by SLC25A1 inhibition (CTPI2-treatment) or octyl-D2HG-treatment in NCI-H460 cell line.

NCI-H460 cells were exposed to 0Gy(**a**), 30Gy(**b,c**), 5Gy(**d**), or 0-8Gy(**e**) alone or with CTPI2 (200µM)-, octyl-D2HG (150µM)- pre-treatment for 2h. **a)** DNA damage was quantified by alkaline comet assay 24h in CTPI2, octyl-D2HG- or non- treated NCI-H460 cells without IR. **b, c)** DNA damage was measured by alkaline comet assay 6h (b) or 24h (c) in CTPI2, octyl-D2HG- or non- treated NCI-H460 cells upon IR with a dose of 30Gy. **d)** γ-H2AX signal was assessed by flow cytometry 6h after combinatory treatment of IR (5Gy) and CTPI2, octyl-D2HG- or non-treatment. **e)** Colony formation assay was used to verify the survival fraction of NCI-H460 cells upon CTPI2- and octyl-D2HG-treatment in combination with IR. Data represent the mean values (±SEM) from three independent experiments (N=3). Statistical significance: one way ANOVA followed by Bonferroni posttest. ns=not significant ($p > 0.05$), * $p < 0.05$, *** $p < 0.001$, **** $p < 0.0001$.

3.3 CTPI2 disrupted cell function

Repair of DNA damage is fundamental for cell survival. As shown above, CTPI2- and octyl-D2HG-treatment were interfering with DNA repair processes. To gain deeper insight of their effect on cell physiology, flow cytometry was employed to explore their effects on other cell functions. Here, I further concentrated on NCI-H460 cell line for the following functional and mechanistic analysis, since further data was already available or is in the process of evaluation with this cell line (e.g. metabolomics analysis). First, I determined cytosolic ROS production by staining the cells with DHE. CTPI2-treatment stimulated cytoplasmic ROS production compared with non-treated control NCI-H460 cells, no matter with or without IR-treatment (Figure 8a). The comparison between non-irradiated (0Gy) controls and irradiated NCI-H460 cells with a dose of 5Gy without additional pharmacological treatment, indicated that IR could generate ROS in cytoplasm of NCI-H460 cells, which was consistent with previous results (Tominaga et al., 2004). Interestingly, octyl-D2HG-treatment led to comparable cytoplasmic ROS-levels as CTPI2 exposure. Next, ROS-levels in mitochondria were explored by using MitoSOX staining and flow cytometry. Here, quantification of MitoSOX positive cells in flow cytometry allow for assessment of mitochondrial ROS-levels. Again, CTPI2- or octyl-D2HG treatment with or without IR increased mitochondrial ROS levels, hinting to general cellular oxidative stress induced by CTPI2- or octyl-D2HG-treatment (Figure 8b).

Since SLC25A1 is involved in redox and energy homeostasis (Wang et al., 2013), the ratio of NAD^+/NADH and $NADP^+$/NADPH was monitored. In agreement with increased cytosolic and mitochondrial ROS levels, CTPI2-treatment increased the ratio of NAD^+/NADH and $NADP^+$/NADPH, indicating a more oxidative state of NCI-H460 cells (Figure 8c, d). Similar results could be revealed with octyl-D-2HG treatment (Figure 8c, d). What's more, investigating the relative amount of NAD^+, NADH, $NADP^+$, NADPH, revealed that both CTPI2 and octyl-D2HG, could reduce the amount of these metabolites (Figure 8e, f).

I also analyzed apoptosis and cell death levels by flow cytometry using determination of cells in the apoptotic sub G1 fraction (Nicoletti *et al.*, 1991) and the fraction of dead cells using propidium iodide (PI) exclusion . CTPI2- or octyl-D-2HG-treatment for 48 h was inducing higher apoptosis (Figure 8g) and cell death levels (Figure 8h) in NCI-H460 cells

compared to untreated controls. Furthermore, combining CTPI2- or octyl-D-2HG-treatment with IR increased apoptosis and cell death levels in NCI-H460 cells (Figure 8g, h).

Previous work in my group demonstrated an involvement of SLC25A1 in mitochondrial energy metabolism. I therefore explored the impact of D-2HG, induced by SLC25A1-inhibition, on the mitochondrial function by using Seahorse XF96 Extracellular Flux analyzer. The utilization of mitochondrial stress test revealed that both CTPI2- and octyl-D2HG-treatment for 24h inhibited basal respiration, maximal respiration and ATP production of mitochondria, with or without additional IR-treatment (Figure 8i-k).

Finally, I determined the effect of the treatments on cell proliferation and viability by the crystal violet assay. In agreement with functional analysis above, proliferation of NCI-H460 cells was slightly reduced 24h after CTPI2- or octyl-D-2HG-treatment (Figure 8l). Taken together, CTPI2- or octyl-D-2HG-treatment affected short-term proliferation and survival of NCI-H460 cells by lowering mitochondrial function and shifting the balance of the co-Enzymes and energy carrier-molecules NAD and NADP to an oxidative state, with decreasing the relative amount of NAD+, NADH, NADP+, and NADPH compared to non-treated control.

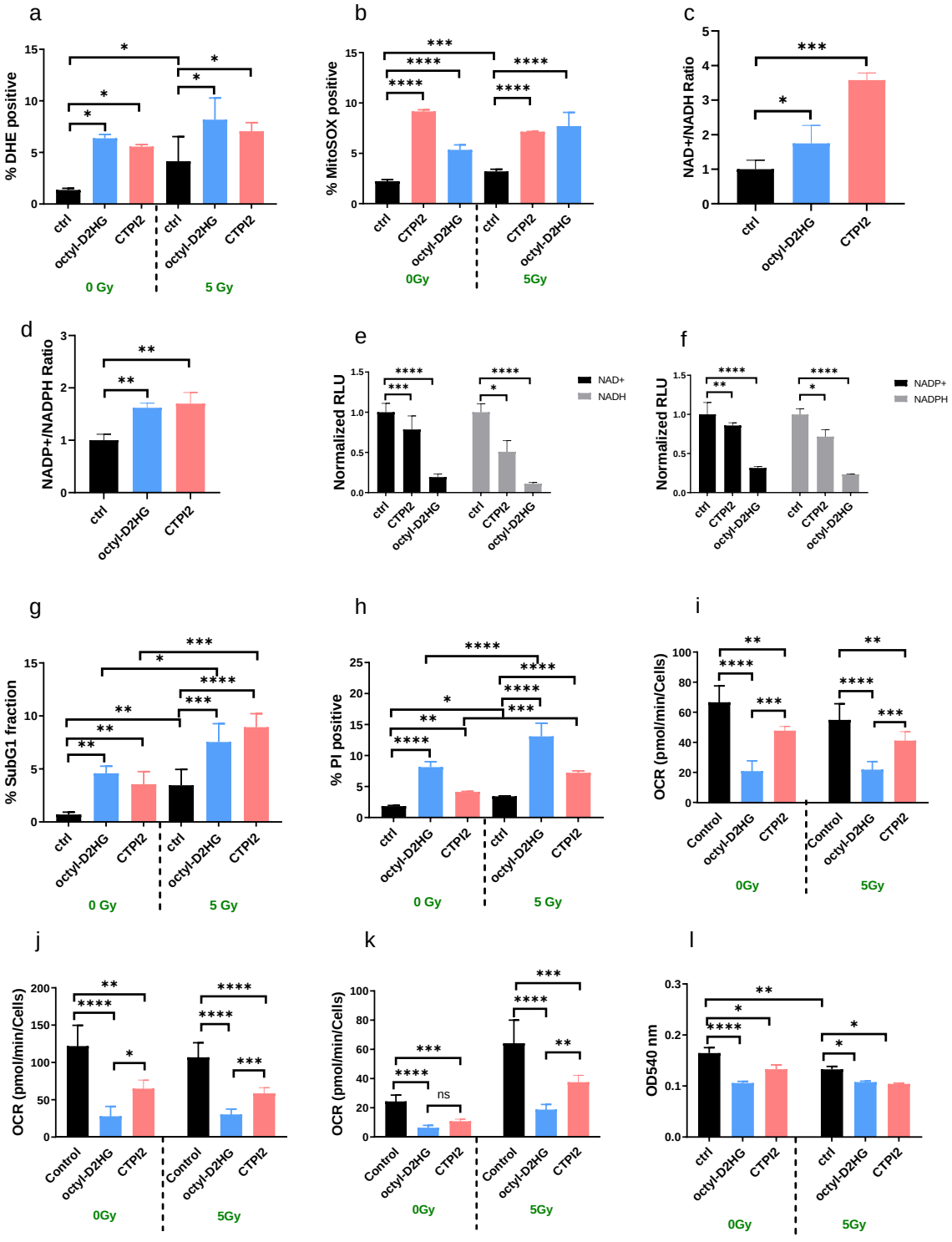
a
% DHE positive
ctrl
octyl-D2HG
CTPI2
0 Gy
5 Gy
b
% MitoSOX positive
0Gy
5Gy
c
NAD+/NADH Ratio
d
NADP+/NADPH Ratio
e
Normalized RLU
NAD+
NADH
f
NADP+
NADPH
g
% SubG1 fraction
h
% PI positive
i
OCR (pmol/min/Cells)
Control
j
k
ns
l
OD540 nm

Figure 8: SLC25A1 inhibition by CTPI2-treatment or octyl-D2HG altered cell metabolism, viability and function in NCI-H460 cell line.

NCI-H460 cells were treated with CTPI2 (200μM), octyl-D2HG (150μM) or non-treatment, combined with 0Gy **(a-l)** and 5Gy **(a-b, g-l)**. **a,b)** NCI-H460 cells were stained with DHE **(a)** or mitoSOX **(b)** 6h after treatment to detect cytoplasmic **(a)** or mitochondrial **(b)** ROS levels with flow cytometry. **c-f)** NAD and NADP kits were utilized to determine the ratio of NAD+/NADH **(c)**, NADP+/NADPH **(d)** and the relative amounts of NAD+, NADH **(e)**, NADP and NADPH **(f)** in NCI-H460 cells 24h after treatment. **g)** Apoptosis was determined 48h after treatment by staining the cells with propidium iodide (PI) in a hypertonic citrate buffer and subsequent analysis of the Sub-G1 fraction by using flow cytometry. **h)** Cell death levels were investigated by flow cytometry quantifying the % of PI-positive cells representing the fraction of dead cells 48h after treatment. **i-k)** Mitochondrial function was measured 24h after treatment by Seahorse XF96 Extracellular Flux analyser with the utilization of mitochondrial stress test. Mitochondrial function, including basal respiration **(i)**, maximal respiration **(j)** and ATP production **(k)**, were measured 24h after CTPI2 or octyl-D2HG treatment, with or without IR. **l)** Crystal violet assay was applied to determine cell proliferation and viability 24h after CTPI2 or octyl-D2HG treatment, with (5Gy) or without (0Gy) IR. Data represent the mean values (±SEM) from three independent experiments (N=3). Statistical significance: one way ANOVA followed by Bonferroni post-test. ns=not significant ($p > 0.05$), * $p < 0.05$, ** $p < 0.01$, *** $p < 0.001$, **** $p < 0.0001$.

3.4 CTPI2 could inhibit tumor growth and sensitize to EJ-inhibitors treatment *in vivo*

Preliminary data in my group suggested that treatment with CTPI2 enhances sensitivity to inhibitors of end-joining (EJ)-pathways (e.g., Poly ADP Ribose Polymerase (PARP) or DNA-dependent protein kinase, catalytic subunit (DNAPKcs)), pointing to the induction of a HR-ness phenotype. The *in vitro* validation of CTPI2-induced sensitivity to inhibitors of EJ-pathways had been performed by Christian Kalthoff (MD-thesis to be submitted) using long-term colony formation assays. In the present thesis, I employed a well described Chick Embryo Chorioallantoic Membrane (CAM) model established for studying tumor growth, invasion and metastasis (Ribatti, 2016) as a proof-of-concept platform for validation of CTPI2-induced sensitivity to PARP-inhibition in NCI-H460 cancer cells *in vivo*. Treatment of NCI-H460 cells with CTPI2 alone significantly reduced tumor volume (Figure 9a and 9b). Combination of CTPI2 with a single dose of 5Gy potentiated the effect by significantly reducing the tumor volume compared to the single treatments (Figure 9a and 9b). Combining CTPI2 with the PARP inhibitor-PJ34 reduced the tumor volume of irradiated NCI-H460 cells compared to single drug treatments in combination with IR. These data corroborate the findings obtained from the long-term colony formation assays obtained by C. Kalthoff.

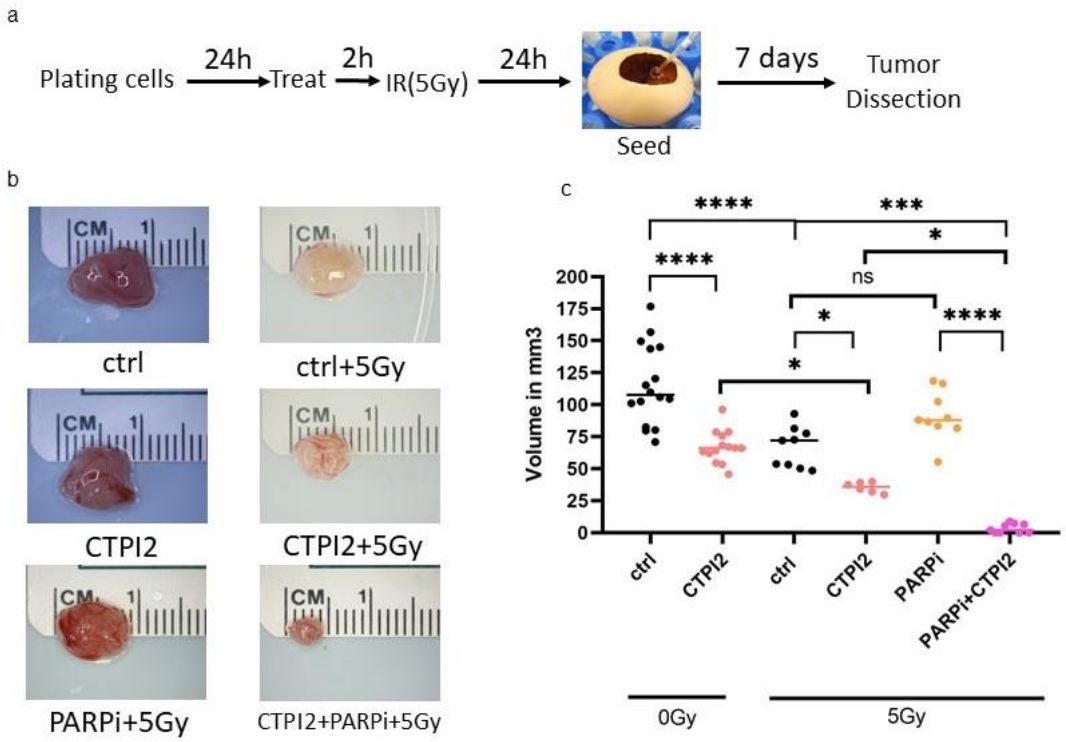

Figure 9: SLC25A1 inhibition by CTPI2-treatment reduced tumor growth *in vivo*, which was further enhanced when combined with PARP inhibition (PARPi) under the condition of IR.

a) NCI-H460 cells were plated in flasks 24h before CTPI2 (200µM), PARPi (PJ34 at 4µM) or CTPI2+PARPi treatment. Cells were irradiated with a dose of 5Gy 2h after drug-treatment or stayed without IR. After 24h, cells were detached from the flask and grafted onto the chicken chorioallantoic membrane (CAM) of the eggs. Tumors were dissected 7 days after grafting. **b)** Exemplary photos of tumors dissected from CAM model 7 days after grafting. NCI-H460 cells were treated with CTPI2 (200µM) and PARPi (PJ34 at 4µM) in combination with (5Gy) or without (0Gy) IR before grafting to the egg. **c)** Quantification of tumor volumes obtained in represented treatment groups. Data represent the median values from three independent experiments (N=3). Statistical significance: one way ANOVA followed by Bonferroni post-test. ns $p > 0.05$, * $p < 0.05$, *** $p < 0.001$, **** $p < 0.0001$.

3.5 α-ketoglutarate (αKG) reinforced the effect of CTPI2

So far my results indicated that radiosensitization of cancer cells by CTPI2-mediatd inhibition of SLC25A1 involves metabolic reprogramming with accumulation of D-2HG. Since D-2HG acts as competitive inhibitor of αKGDD replacing αKG as a substrate, (reviewed by Xiang *et al.*, 2020) (Figure 3), I hypothesized that αKG supplementation upon CTPI2-treatment could reverse or save observed effects induced upon CTPI2 or octyl-D2HG-treatment. Therefore, I first explored the effect of αKG supplementation on

D-2HG production. As depicted in Figure 10b, αKG-treatment alone hardly modulated D-2HG production. Surprisingly, αKG treatment significantly enhanced D-2HG accumulation in response to CTPI2 treatment (Figure 10b). Based on the combinatorial effect of αKG and CTPI2-treatment on D-2HG production, I subsequently analysed the effects of combined CTPI2- and αKG-treatment on the biological activity of NCI-H460 cells in more detail. Consistent with the increased accumulation of D-2HG, αKG enhanced CTPI2's effect on radiation-induced DNA damage 6h after treatment as determined by the alkaline Comet assay (Figure 10c). Furthermore, αKG also potentiated radiation-induced DNA damage upon octyl-D2HG-treatment (Figure 10c). These findings support our hypothesis of negative regulation of DNA damage repair by increased D-2HG accumulation. What's more, combined treatment with CTPI2 and αKG further enhanced the γ-H2AX signal induced by CTPI2 treatment and IR (Figure 10d). Nevertheless, increased levels of radiation-induced γ-H2AX foci by octyl-D2HG at 6h post-irradiation were not further augmented by αKG supplementation. (Figure 10d).

Next, I explored the effects of αKG-treatment upon CTPI2- or octyl-D2HG-treatment, in addition to the previously obtained results presented in figure 8, with or without IR. Here, I collected additional data on cellular parameters assessing ROS, apoptosis, cell death levels as well as mitochondrial function upon αKG-supplementation in combination to CTPI2- or octyl-D2HG-treatment with or without IR. Cell function was investigated with or without IR to better understand the role of IR. Analysis of cytoplasmic ROS levels by flow cytometry 6h after treatment revealed highest increase in ROS-levels upon combinatory treatment of αKG and octyl-D2HG without IR in NCI-H460 cells. Similar tendency to increased ROS levels was also observed upon combinatory treatment with CTPI2 and αKG, though with lower absolute levels of ROS-positive cells. When adding IR, the effect of combinatory treatment of NCI-H460 cells with αKG and CTPI2 or octyl-D2HG and αKG was contrary to that without IR (Figure 10e). In more detail, combing CTPI2 and αKG-treatment with a single dose IR of 5Gy increased ROS levels in NCI-H460 cells, whereas no effect observed with combination of octyl-D2HG and αKG treatment (Figure 10e). While assessing apoptosis levels, αKG-treatment only potentiated the CTPI2's impact on cells without IR, whereas addition of IR had no additional effect (Figure 10f). Adding IR to the combinatory treatments did not significantly increase apoptosis levels compared to non-irradiated but drug-treated cells (Figure 10f). Next, cell

death levels were measured by using flow cytometry as described above (3.3). Here, αKG enhanced cell death levels induced by CTPI2-treatment alone with or without IR, which was not observed by replacing CTPI2 by octyl-D2HG treatment. It was intriguing to discover that treatment with αKG influenced cell death levels in NCI-H460 cells when combined with IR, whereas αKG was not cytotoxic without IR (Figure 10g). Since CTPI2 exerts its function on the mitochondrial citrate carrier, the mitochondrial function was measured by using extracellular flux analyser (Seahorse-Analyzer). Here, treating the NCI-H460 cancer cells with αKG and CTPI2 for 24h reduced basal mitochondrial respiration with or without IR (Figure 10h). Interestingly, octyl-D2HG-treatment alone exerted strong effects on basal mitochondrial respiration without and 24h after IR-treatment (Figure 10h). However, additional αKG-treatment had no supplementary effect on mitochondrial function as in case of octyl-D2HG. Additionally, αKG-treatment in combination with CTPI2 further reduced cell viability/proliferation of NCI-H460 cells with or without IR (Figure 10i) 24h after treatment. Again, αKG in combination with octyl-D2HG did not further reduce cell viability/proliferation.

Taken together, the combination treatment with αKG and CTPI2 potentiated the basal mitochondrial respiration defect compared to CTPI2-treatment alone with or without IR, thus influencing ROS and cell death levels of NCI-H460 cells upon IR. Such effects were not observed for octyl-D2HG-treatment (Figure 10).

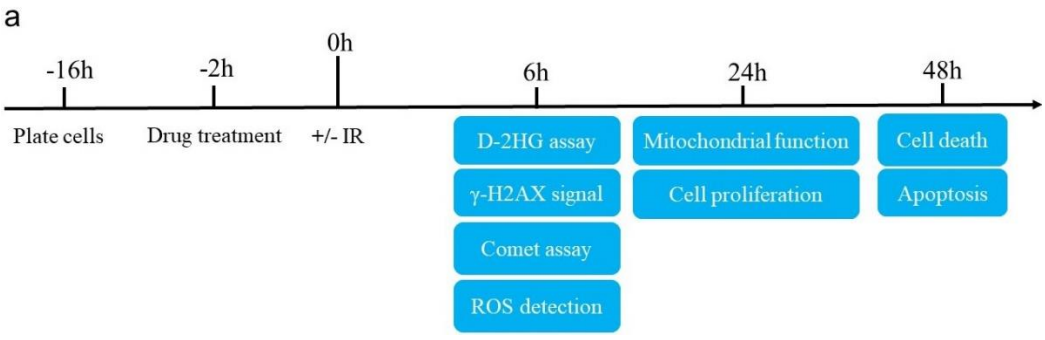

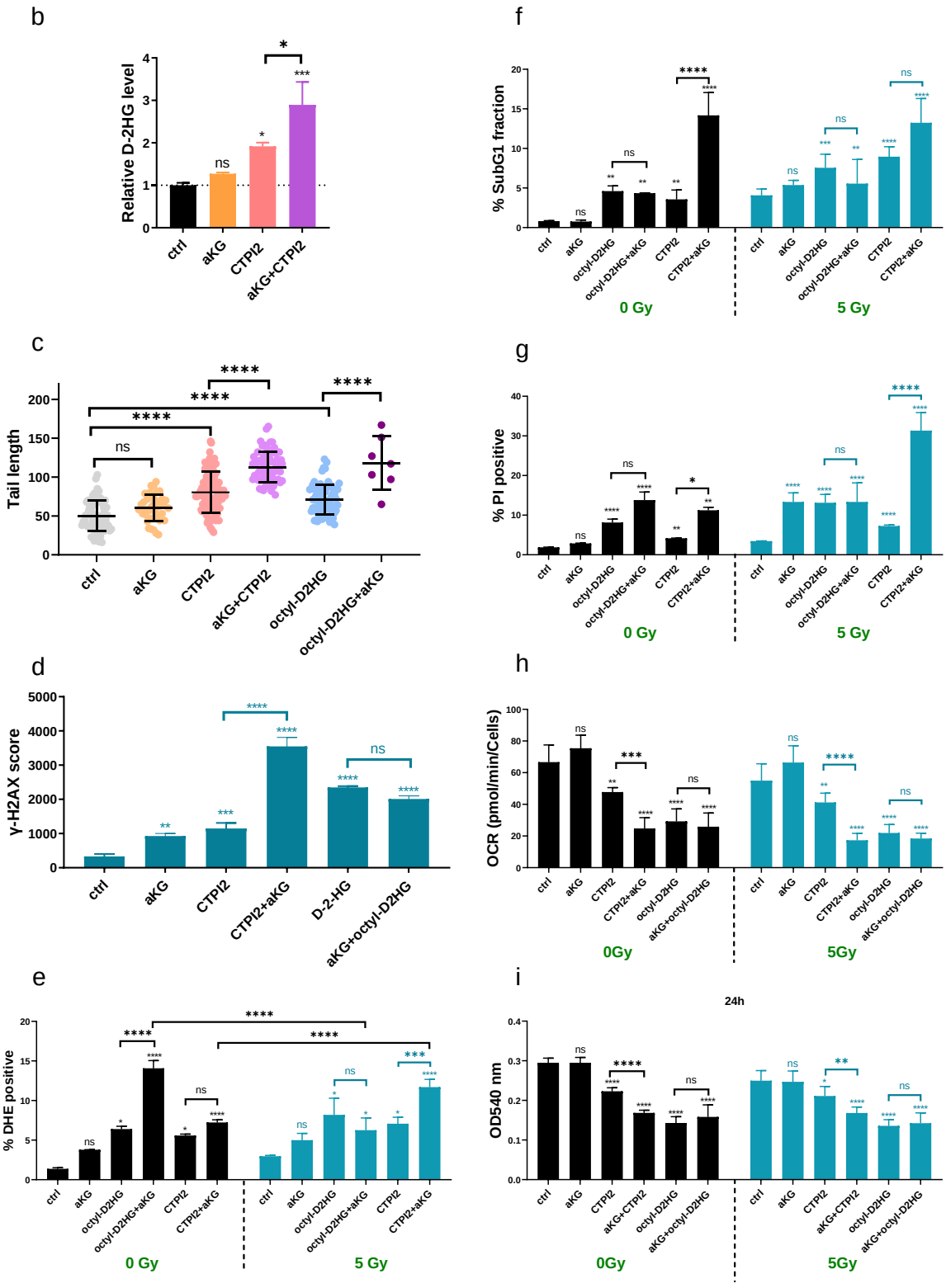
b
Relative D-2HG level
ctrl
aKG
CTPI2
aKG+CTPI2
f
% SubG1 fraction
ctrl
aKG
octyl-D2HG
octyl-D2HG+aKG
CTPI2
CTPI2+aKG
0 Gy
5 Gy
c
Tail length
ctrl
aKG
CTPI2
aKG+CTPI2
octyl-D2HG
octyl-D2HG+aKG
g
% PI positive
0 Gy
5 Gy
d
γ-H2AX score
ctrl
aKG
CTPI2
CTPI2+aKG
D-2-HG
aKG+octyl-D2HG
h
OCR (pmol/min/Cells)
ctrl
aKG
CTPI2
CTPI2+aKG
octyl-D2HG
aKG+octyl-D2HG
0Gy
5Gy
e
% DHE positive
ctrl
aKG
octyl-D2HG
octyl-D2HG+aKG
CTPI2
CTPI2+aKG
0 Gy
5 Gy
i
24h
OD540 nm
ctrl
aKG
CTPI2
aKG+CTPI2
octyl-D2HG
aKG+octyl-D2HG
0Gy
5Gy

Figure 10: αKG-treatment potentiated the effect induced by CTPI2.

a) Schematic representation of the experimental timeline. NCI-H460 cells were exposed to treatment with αKG (8mM), CTPI2 (200μM), octyl-D2HG (150μM), or the combination of αKG and CTPI2, αKG and octyl-D2HG for 2h before IR- or sham-IR- treatment. Subsequent analyses were as follows: **b)** D-2HG production (D-2HG assay kit) 6h after treatment, **c)** DNA damage (alkaline Comet assay) 6h after treatment with 30Gy IR, **d)** γ-H2AX signal assessed by flow cytometry 6h after treatment with 5Gy IR, **e)** cytoplasmic ROS levels with DHE staining measured by flow cytometry 6h post-treatment, **f,g)** apoptosis and cell death levels were investigated by flow cytometry using determination of cells in the apoptotic sub G1 fraction and the fraction of dead cells using propidium iodide (PI) exclusion 48h after treatment. **h)** Mitochondrial basal respiration was measured 24h after treatment by Seahorse XF96 Extracellular Flux analyzer with the utilization of mitochondrial stress test. **i)** cell proliferation and viability with the utility of crystal violet assay 24h post-treatment. Data represent the mean values (±SEM) from three independent experiments (N=3). Statistical significance: by non-parametric unpaired t-test. ns $p > 0.05$, * $p < 0.05$, ** $p < 0.01$, *** $p < 0.001$, **** $p < 0.0001$.

3.6 CTPI2's effect could be counteracted by nicotinamide (NAM)

As demonstrated in section 3.3 I observed that the ratio of NAD^+/NADH was altered by CTPI2- or octyl-D2HG treatment (Figure 8c). Since nicotinamide (NAM) is the precursor of NAD^+, it may have the potential to reverse the ratio of NAD^+/NADH and thus modify cell metabolism (Buque et al., 2021; Kirkman and Gaetani, 1984). I therefore hypothesized that feeding of the NCI-H460 cells with NAM could restore the decline in NAD+ levels observed upon CTPI2 or octyl-D2HG-treatments and thus rescue radiation-induced DNA damage. Assessing the DNA damage, by measuring γ-H2AX signal by flow cytometry, revealed that addition of NAM to CTPI2-, octyl-D2HG- or CTPI2+αKG-treated NCI-H460 cells alleviated radiation-induced DNA damage, but no effect observed on the untreated control or αKG-treated group (Figure 11a). In addition to DNA damage, NAM treatment also counteracted the effect of CTPI2-treatment or the combination treatment of CTPI2 and αKG on cytoplasmic ROS levels (Figure 11b). However, NAM-treatment only reduced the apoptosis levels in CTPI2-treated and in CTPI2+αKG-treated NCI-H460 cells (Figure 11c), but not in octyl-D2HG-, octyl-D2HG+αKG-, αKG- or non-treated groups. Interestingly, NAM-treatment revealed a trend to reducing cell death levels in only CTPI2-treated group ($p = 0.53$) but only reached statistical significant differences in cells treated with octyl-D2HG+αKG and CTPI2+αKG (Figure 11d). By contrast, the destructive effect of octyl-D2HG or octyl-D2HG+αKG on the cell function

could not be constantly abrogated by NAM supplementation compared to CTPI2 or CTPI2+αKG treatment groups.

Although the results of cytoplasmic ROS generation and apoptosis induction of NAM supplementation to octyl-D2HG or octyl-D2HG+αKG were similar to that of CTPI2 or CTPI2+αKG, the apoptosis induction showed slightly stronger effects when octyl-D2HG or octyl-D2HG+αKG were combined with NAM treatment (Figure 11b-d).

In addition, I tested potential beneficial effects of NAM supplementation upon CTPI2 or octyl-D2HG-treatments on the basal mitochondrial function by using extracellular flux analyser. As illustrated in Figure 11e, NAM-treatment for 24h recuperated the basal mitochondrial respiration almost to the level of untreated control group, which was inhibited in CTPI2 or CTPI2+αKG-treated NCI-H460 cells. In contrast, the destructive effect of octyl-D2HG or octyl-D2HG+αKG on the reduction of basal mitochondrial respiration could not be abrogated by NAM supplementation (Figure 11e).

Furthermore, cell proliferation/viability analysis assessed by crystal violet assay further validated differences of NAM supplementation on CTPI2- and octyl-D2HG-treated NCI-H460 cells. In this study, reduced cell viability/proliferation induced by CTPI2 or CTPI+αKG-treatment could be rescued by NAM-supplementation. However, no significant rescue effect by NAM supplementation was observed in octyl-D2HG or octyl-D2HG+αKG treated groups (Figure 11f).

a

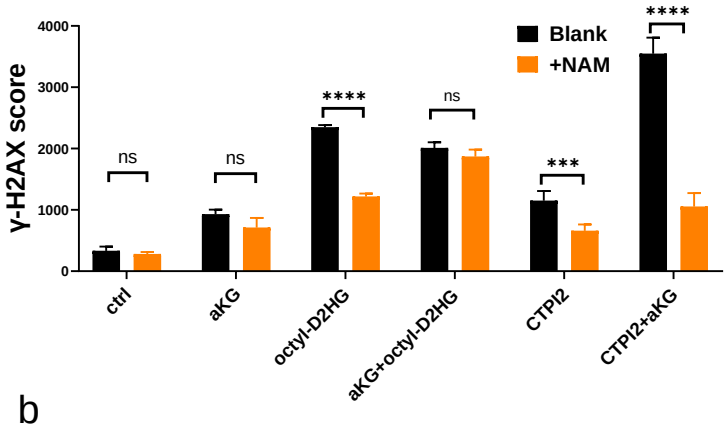
γ-H2AX score
4000
3000
2000
1000
0
Blank
+NAM
ns
ns
****
ns
***
****
ctrl
aKG
octyl-D2HG
aKG+octyl-D2HG
CTPI2
CTPI2+aKG

b

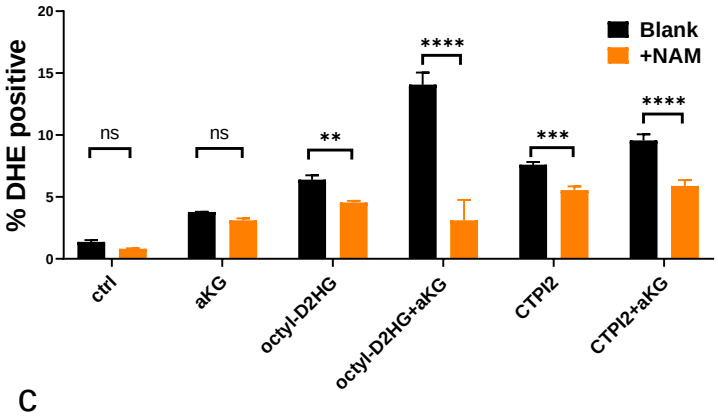
% DHE positive
20
15
10
5
0
Blank
+NAM
ns
ns
**
****
***
****
ctrl
aKG
octyl-D2HG
octyl-D2HG+aKG
CTPI2
CTPI2+aKG

c

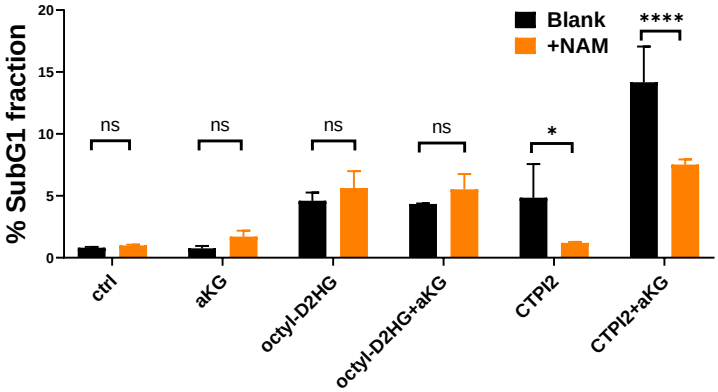
% SubG1 fraction
20
15
10
5
0
Blank
+NAM
ns
ns
ns
ns
*
****
ctrl
aKG
octyl-D2HG
octyl-D2HG+aKG
CTPI2
CTPI2+aKG

d

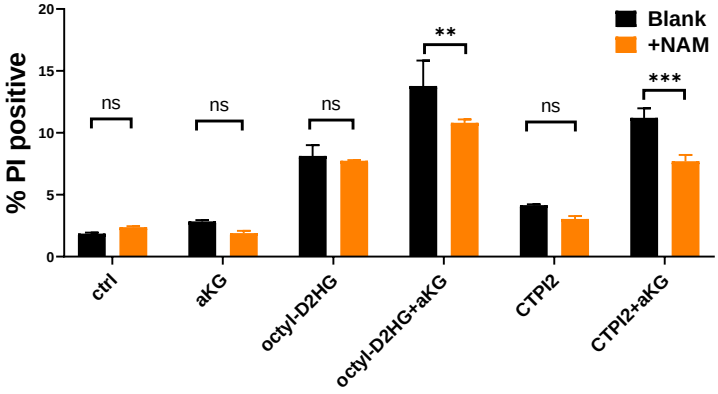
% PI positive
20
15
10
5
0
Blank
+NAM
ns
ns
ns
**
ns
***
ctrl
aKG
octyl-D2HG
octyl-D2HG+aKG
CTPI2
CTPI2+aKG

e

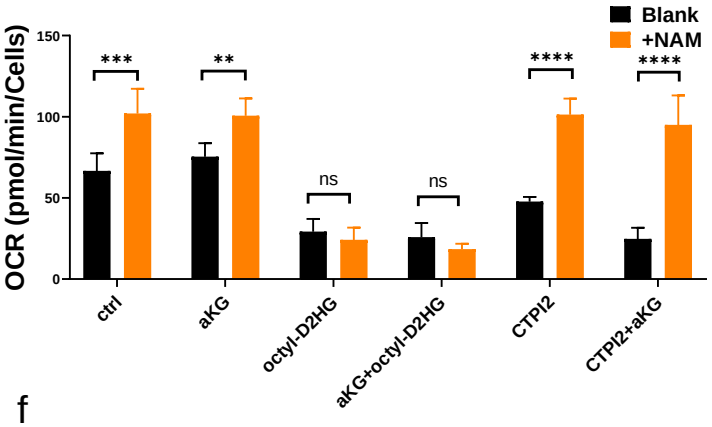
Blank
+NAM
OCR (pmol/min/Cells)
150
100
50
0
***
**
ns
ns
****
****
ctrl
aKG
octyl-D2HG
aKG+octyl-D2HG
CTPI2
CTPI2+aKG

f

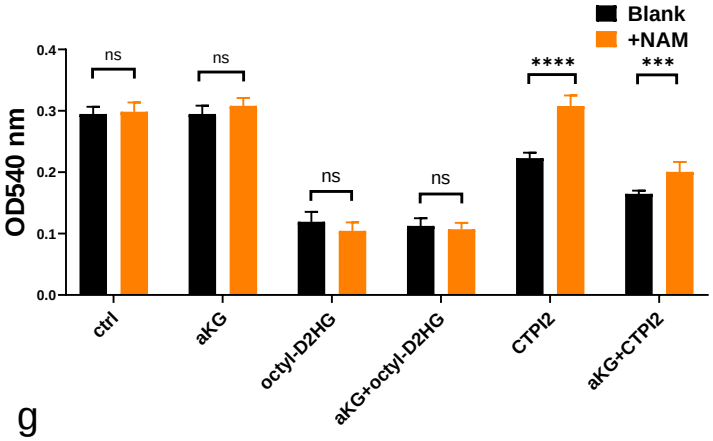
Blank
+NAM
OD540 nm
0.4
0.3
0.2
0.1
0.0
ns
ns
ns
ns
****
***
ctrl
aKG
octyl-D2HG
aKG+octyl-D2HG
CTPI2
aKG+CTPI2

g

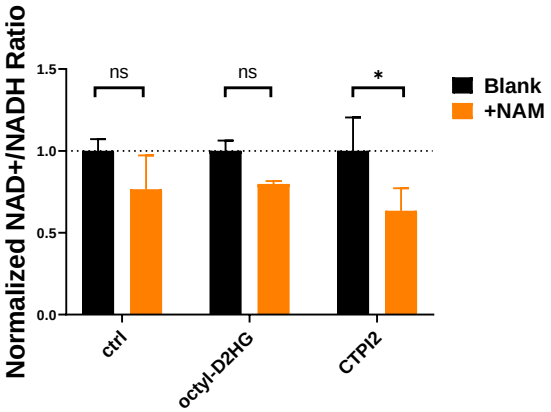
Normalized NAD+/NADH Ratio
1.5
1.0
0.5
0.0
ns
ns
*
Blank
+NAM
ctrl
octyl-D2HG
CTPI2

Figure 11: Nicotinamide (NAM) counteracted the effect induced by CTPI2 treatment.

a) γ-H2AX signal was evaluated at 6h timepoint by flow cytometry after pre-treatment of NCI-H460 cells for 2h with αKG (8mM), CTPI2 (200µM), octyl-D2HG (150µM), αKG+CTPI2, or αKG+octyl-D2HG treatment in combination with or without NAM (1mM) supplementation and subsequent IR with a dose of 5Gy. **b)** NAM treatment on cytoplasmic ROS (% DHE-positive cells) measured by flow cytometry and stimulated by CTPI2-, octyl-D2HG-, CTPI2+αKG- or octyl-D2HG+αKG- treatment for 6h in NCI-H460 cell line. **c)** % sub-G1 fraction obtained by PI-staining of cells in a hypertonic buffer and subsequent analysis by flow cytometry. The apoptosis (% sub-G1 fraction) levels induced by NAM in addition to CTPI2-, octyl-D2HG-, CTPI2+αKG- or octyl-D2HG+αKG- treatment for 48h in NCI-H460 cell line. **d)** Cell death measured as % of PI-positive cells in flow cytometry 48h after treatment in NCI-H460 cell line. **e)** Basal respiration (oxygen consumption rate, OCR) measured 48h by Seahorse XFe analyser after CTPI2-, octyl-D2HG-, CTPI2+αKG- or octyl-D2HG+αKG- treatment with or without NAM supplementation in NCI-H460 cell line. **f)** Cell proliferation obtained by crystal violet assay quantifying the OD_{540} -values 24h after CTPI2-, octyl-D2HG-, CTPI2+αKG- or octyl-D2HG+αKG- treatment with NAM supplementation in NCI-H460 cell line. **g)** The ratio of NAD+/NADH was normalized to respective treatments without NAM supplementation to visualize the effect of additional NAM treatment. Data represent the mean values (±SEM) from three independent experiments (N=3). Statistical significance: by non-parametric unpaired t-test. ns $p > 0.05$, * $p < 0.05$, ** $p < 0.01$, *** $p < 0.001$, **** $p < 0.0001$.

3.7 Inhibition of Histon-lysin-demethylases (KDMs) recapitulated the effects observed upon SLC25A1 inhibition by CTPI2.

So far, my data indicated that inhibition of SLC25A1 by CTPI2 stimulated substantial D-2HG accumulation (Figure 6) and this effect is associated with induction of DNA damage and potent radiosensitization (Figure 7). It has been found that D-2HG accumulation impacts the function of Histone-lysin demethylases 4B (KDM4B), a subgroup of αKGDDs, and thereby affects proper DNA repair by HR by disrupting local chromatin signalling(Sulkowski et al., 2020). Based on this observation, I wondered whether KDM inhibition could recapitulate the functional phenotype induced by CTPI2 treatment. In order to mimic the inhibiting effect of CTPI2 on KDM, I treated NCI-H460 cells with JIB-04, a pan-inhibitor of KDMs. Similar to CTPI2's effect, JIB-04-treatment stimulated radiation-induced γ-H2AX formation, which was further enhanced by additional αKG supplementation (Figure 12a). Accordingly, JIB-04-treatment for 6h stimulated cytoplasmic ROS-levels, apoptosis levels and cell death levels of NCI-H460 cells without IR at 24h after treatment, respectively (Figure 12b-d). These effects were significantly enhanced when adding αKG. When the cells were treated with IR besides drug treatment, similar augmentation effect on ROS and cell death levels upon αKG+JIB-04 treatment

was noted (Figure 12b-d). As an exception, the apoptosis levels were not significantly altered upon the described treatments (Figure 12c). However, cell viability/proliferation was remarkably inhibited after 24h treatment with JIB-04, and the effect was more pronounced when combined with αKG treatment, no matter with or without IR (Figure 12e).

Taken together, the above results reveal comparable effects on increased γH2A.X foci induction at 6h, ROS and cell death induction upon JIB-04-treatment compared to CTPI2 treatment. Of note, that especially the combination effect αKG with CTPI2 or JIB-04 treatment was reproducible, hinting to JIB-04 as one target of cellular metabolic reprogramming induced by CTPI2 treatment.

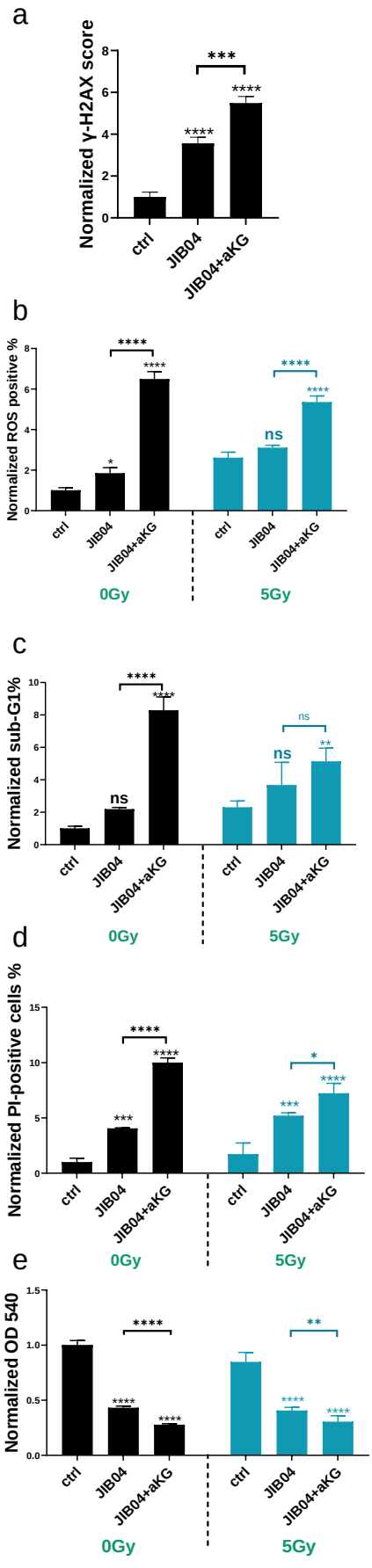
a
Normalized γ-H2AX score
***
****
****
ctrl
JIB04
JIB04+aKG
b
Normalized ROS positive %
****
****
*
****
****
ns
ctrl
JIB04
JIB04+aKG
ctrl
JIB04
JIB04+aKG
0Gy
5Gy
c
Normalized sub-G1%
****
****
ns
ns
ns
**
ctrl
JIB04
JIB04+aKG
ctrl
JIB04
JIB04+aKG
0Gy
5Gy
d
Normalized PI-positive cells %
****
****
***
*
***
****
ctrl
JIB04
JIB04+aKG
ctrl
JIB04
JIB04+aKG
0Gy
5Gy
e
Normalized OD 540
****
**
****
****
****
ctrl
JIB04
JIB04+aKG
ctrl
JIB04
JIB04+aKG
0Gy
5Gy

Figure 12: Inhibition of Histone-lysine-demethylases (KDMs) recapitulated the effects observed upon SLC25A1 inhibition by CTPI2.

a) γ-H2AX signal was evaluated at 6h timepoint by flow cytometry after 2h pre-treatment with JIB-04 (1μM)- or αKG (8mM) +JIB-04- and subsequent IR with 5Gy in NCI-H460 cells. **b)** JIB-04- or αKG+JIB-04- treatment on cytoplasmic ROS (% DHE-positive cells) was measured by flow cytometry 6h after IR (5Gy) or without IR(0Gy) in NCI-H460 cell line. **c)** Apoptosis levels (% sub-G1 fraction) induced by JIB-04- or αKG+JIB-04- treatment for 48h after IR(5Gy) or without IR(0Gy) in NCI-H460 cell line. % sub-G1 fraction obtained by PI-staining of cells in a hypertonic buffer and subsequent analysis by flow cytometry. **d)** Cell death measured as % of PI-positive cells in flow cytometry 48h after IR(5Gy) or without IR(0Gy) in NCI-H460 cell line. **e)** Cell proliferation/viability quantified 24h after JIB-04- or αKG+JIB-04- treatment with IR(5Gy) or without IR(0Gy) in NCI-H460 cell line. Data represent the mean values (±SEM) from three independent experiments (N=3). Statistical significance: by non-parametric unpaired t-test. ns $p > 0.05$, * $p < 0.05$, ** $p < 0.01$, *** $p < 0.001$, **** $p < 0.0001$.

4 Discussion

Tumor metabolism has been standing under the spotlight of cancer research for decades (Pavlova and Thompson, 2016). With the rapid development of methodology and technology, new discoveries which compensate traditional theories are also fulfilling the big picture of cancer study (Reinfeld *et al.*, 2021). As a new field of investigation, the development of collaborating strategies which combine RT with drugs targeting phenotype-specific metabolic vulnerabilities has been proposed to enhance the cancer cell lethality of RT and to overcome radioresistance associated with metabolic deregulation(Matschke et al., 2021; Sitthideatphaiboon et al., 2021).

It has already been reported by my group and others that genetic (siRNA) or pharmacologic targeting of SLC25A1 by BTA, results in accumulation of the D-enantiomers of 2-HG under different circumstances (Hlouschek *et al.*, 2018a). In the present thesis, I further validated the induction of D-2HG by using the more specific small molecule inhibitor of SLC25A1, CTPI2, in NCI-H460 lung cancer cells. The obtained results revealed a stable and time-dependent D-2HG induction upon CTPI2-treatment from 6 to 48 hours after treatment (Figure 6a). Next, a potential role of D-2HG accumulation on DNA damage induction, mitochondrial function, short-term ROS and cell death levels were explored by treating the NCI-H460 cell line with octyl-D2HG instead of the D-2HG inducer CTPI2. These data clearly indicated that octyl-D2HG mimicked the induction of cellular processes which were important to cancer cell survival upon irradiation (Figure 8a, b, g, h). Thus, SLC25A-inhibition by CTPI2 represents a suitable strategy for the induction of D-2HG and thereby to affect mitochondrial energy metabolism and DNA damage repair upon irradiation. Mechanistically, the effects observed upon CTPI2-induced D-2HG accumulation correlated to dependency on NAD^+/NADH and the function of KDMs. In fact, CTPI2 induced an oxidative metabolic state, which was reversed by NAM supplementation (Figure 11g). In contrast to that, the effects of octyl-D2HG could not be reversed by NAM-supplementation, implying that the antineoplastic effect of this surrogate of the oncometabolite D2HG may be mainly based on the inhibition of KDMs. Finally, D-2HG accumulation induced by SLC25A1 inhibition rendered NCI-H460 cells sensitive to PARP-inhibition *in vivo* providing a pharmacologic strategy for induction of a HR-ness phenotype by metabolic reprogramming.

4.1 DNA damage induction and D2HG accumulation

In more detail, DSBs are one of the hazardous consequences of IR, and the repair process requires structural alterations of chromatin (Khanna and Jackson, 2001). The mitochondrial citrate transporter SLC25A1, embedded in the inner mitochondrial membrane, exerts its effects on cell metabolism and on the regulation of chromosome integrity (Morciano et al., 2009). Therefore, it is interesting to explore the potential connection between SLC25A1 and DNA damage along with the DNA damage repair system. Herein, a recent study has illustrated the mechanistic aspect of the link between 2-HG and DSB repair on the level of KDM4B-mediated histone 3 lysine 9 trimethylation (H3K9me3) near DNA breaks (Sulkowski *et al.*, 2020). This study emphasized a pivotal role of 2-HG-mediated suppression of HRR and provided an excellent explanation for the relationship between oncometabolites, the DDR and DSB repair (Sulkowski *et al.*, 2020). In line with this study, the work of the present thesis found that CTPI2 synergized with IR-treatment on DNA damage induction in A549, NCI-H460, U87-MG and T98G cell lines as determined by the alkaline comet assay. The observed synergy corroborated earlier observations on SLC25A1-regulated structural modification of chromatin, which emphasized the various roles of this citrate carrier on genetic modification rather than its action as a single metabolite transporter (Morciano *et al.*, 2009).

In the present thesis, I observed that DNA damage was sustained until 4 hours after IR, which was in harmony with the time-dependent γ-H2AX resolution discovered by Mai et al (Nanya et al., 2015). CTPI2-treatment did not induce DNA damage without IR, but interfered with the repair of radiation-induced DNA damage, highlighting its importance for DNA repair pathways. This led to the conclusion that CTPI2 plays a role as enhancer of IR-toxicity, without inducing DNA damage in non-irradiated cells. Since CTPI2 induced accumulation of the oncometabolite D-2HG, octyl-D2HG was utilized as a surrogate for CTPI2 treatment in order to monitor its effects on radiation-induced DNA damage by the alkaline comet assay. The obtained data again demonstrated that neither CTPI2 nor octyl-D2HG treatment induced DNA damage without IR. However, combining IR-treatment with CTPI2 or octyl-D2HG exerted similar potentiating effects on the level of radiation-induced DNA damage in NCI-H460 cells, compared to IR-treatment alone. Similar results were observed when measuring γ-H2AX by flow cytometry. However, the effect of octyl-D2HG treatment was more pronounced on the

induction of DNA damage compared to CTPI2 treatment. In contrast, CTPI2 treatment in combination with IR reduced the survival of irradiated NCI-H460 cell to a higher extend compared to the octyl-D2HG treatment (Figure 8l). Our data hinted to a pronounced DDR dysregulation induced by CTPI2 compared to octyl-D2HG treatment thus altering the long-term survival of NCI-H460 cancer cells (Figure 7e).

Together with the findings provided by Sulkowski and colleagues (Sulkowski *et al*., 2020) on the role of KDM inhibition for the action of D2HG on affecting the DNA repair processes of HRR and findings in our group on delayed resolution of RAD51-foci upon CTPI2-treatment (MD-thesis of Christian Kalthoff; to be submitted), it was tempting to speculate that disturbance of DNA repair by octyl-D2HG and CTPI2-treatment may mainly be due to altered KDM function (reviewed by Xiang *et al.*, 2020).

4.2 Induction of cellular disfunction

It is important to mention that the generation of free radicals is another important mechanism contributing to IR-induced tumor cell toxicity. IR-induced ROS cause covalent changes in biomolecules and contribute to radiation-related cell death (Spitz et al., 2004). The mechanisms of IR-induced cell death depends on many factors including the cell line, radiation dosage and the state of the cell (Tamulevicius et al., 2007). Some cancer cells, including lung cancer cells, can undergo apoptosis after IR at different doses(Matschke *et al.*, 2016b), though many cells from solid tumors are apoptosis resistant. In this thesis, it was discovered that SLC25A1 inhibition by CTPI2 alone or in combination with IR could gave rise to a higher ROS production in both, the cytoplasm and mitochondria, compared to non-treated NCI-H460 cells. It was therefore intriguing to further explore the effect of CTPI2-treatment and of the induced oncometabolite responsible for its effects, octyl-D2HG-treatment, on cell apoptosis and cell death induction. In non-irradiated NCI-H460 cells, both CTPI2- and octyl-D2HG-treatment promoted apoptosis induction compared to non-treated control cells, which was different from DNA damage induction. However, both treatments induced higher levels of apoptosis in combination with IR compared to IR-treatment alone pointing to suitable use of this treatments in combination with IR. The observation of CTPI2-induced apoptosis was in good accordance with the recent discovery in colorectal cancer, which indicated that knockdown of SLC25A1 significantly inhibited colorectal tumor growth by inducing

apoptosis both *in vitro* and *in vivo* (Yang et al., 2021). Based on ROS production and apoptosis induction, the effect of CTPI2-treatment on cell death was in good harmony with the cell function analysis. Here, octyl-D2HG treatment, as a major oncometabolite responsible for the effects upon SLC25A1-inhibition by CTPI2, exerted comparable effects on ROS, apoptosis and cell death levels of NCI-H460 cancer cells.

4.3 Metabolic reprogramming

Accumulating evidence has suggested that NAD (including NAD+ and NADH) and NADP (including NADP+ and NADPH) could be the active elements which take part in various biological processes, including energy metabolism, mitochondrial function, homeostasis of cellular oxidative state and others (Buque *et al.*, 2021). NADPH is one of the most important factors in cellular antioxidant capacity of numerous metabolic pathways (Kirkman and Gaetani, 1984). NAD+ is an indispensable molecule for energy metabolism and in poly (adenosine 5′-diphosphate-ribose) polymerase (PARP)-related DNA repair process (Canto et al., 2015), both processes are important for recovery from radiation-induced damage. Considering the ROS-triggering effect and DNA repair disturbance induced by SLC25A1i and octyl-D2HG-treatment, it was tempting to speculate that the deep-seated mechanism behind these phenomena may be related to alterations in NAD or NADP metabolites. In consistence with ROS generation results, the ratio of NAD^+/NADH and $NADP^+$/NADPH increased upon CTPI2 or octyl-D-2HG exposure, indicating an oxidative state provoked in NCI-H460 cancer cells upon both treatments. Furthermore, the amount of NAD^+, NADH, $NADP^+$ and NADPH was decreasing after CTPI2 or octyl-D-2HG treatment, suggesting a disturbed balance between generation and consumption of these metabolites upon treatment. As reviewed by Peter Belenky, NAD+ could transform into reduced (NADH), phosphorylated (NADP+) and reduced phosphorylated (NADPH) modes (Belenky et al., 2007). Therefore, it was important to explore treatment-induced changes of the central metabolite, NAD.

Metabolic reprogramming is an inseparable hallmark of cancer (Ward and Thompson, 2012). Clinical study has revealed that SLC25A1 mutation associated with mitochondrial complex V deficiency, which implies that this citrate carrier may interfere with mitochondrial activity (Cohen et al., 2018). Our previous study showed that SLC25A1

inhibition, conducted by 1,2,3-benzene-tricarboxylic acid (BTA), could disturb mitochondria function, in terms of basal respiration, ATP production and spare respiratory capacity (Hlouschek *et al.*, 2018a). Since the mitochondrial ROS had been detected by mitoSOX staining, it was interesting to explore if mitochondrial function was altered by CTPI2 or octyl-D2HG-treatments. Here, a small molecule inhibitor of SLC25A1 (CTPI2) and cell permeable oncometabolite (octyl-D2HG) were used to check their influence on mitochondria function and metabolic reprogramming. The most obvious finding emerged from the analysis was that both CTPI2 and octyl-D2HG-treatments suppressed mitochondrial function significantly compared with non-treated control. Mitochondrial dysfunction observed here was in line with the previous observation that alteration of mitochondrial function was related to ROS overproduction, genomic instability and apoptosis regulation (Yang et al., 2016). Mitochondrial dysfunction has been certified to inhibit tumor progression through disturbing the autophagic machinery, which interacted with NAD+ metabolism through AMPK and mTOR signaling pathways (Zhang et al., 2016). These mitochondrial function analyses broadly supported the observed disbalance of the NAD and NADP metabolite ratio, thus linking NAD^+/NADH and $NADP^+$/NADPH disbalance to mitochondrial dysfunction. This phenomenon of mitochondrial dysfunction and accompanied disbalance of NAD and NADP-levels seems to contribute to the lethal effects induced by CTPI2 or octyl-D2HG on cancer cells.

However, CTPI2 and octyl-D2HG were not completely equivalent in their action on irradiated cancer cells. Particularly, the two treatments differed in the rescue effect on apoptosis, cell death induction, mitochondrial function and cell proliferation by NAM, especially when combined with αKG, respectively.

As explained above, D-2HG is a competitive inhibitor of αKGDD, which uses O_2 and αKG as cofactors to perform a range of oxidation reactions, e.g. modification of chromatin or regulation of protein stability (reviewed by Xiang *et al.*, 2020). It has been reported that αKG is involved in numerous biological processes including anti-oxidative defence, energy production, signalling modules, and genetic modification (Legendre et al., 2020). Additionally, αKG has been used as a nutritional supplement and therapeutic agent, which means it has been examined and approved for clinical use. Here, in the

purpose of counterbalancing the effect of 2-HG, αKG was applied in our study. Surprisingly, αKG promoted CTPI2-induced D-2HG production whereas αKG-treatment alone was unable to increase the concentration of D-2HG by itself. The primary source for 2-HG production is αKG (Intlekofer *et al.*, 2015). However, αKG-treatment was not capable of stimulating the production of D-2HG, implying the reaction conditions didn't meet the requirements for D-2HG generation. However, the combination of CTPI2 and αKG exceeded the influence of CTPI2 alone on D-2HG production, indicating that αKG enhanced CTPI2's ability or CTPI2-treatment provided necessary conditions for 2-HG production enhanced by αKG. To further explore the effect of αKG and CTPI2 treatment on cell biological activities, these combinatory treatments was tested to investigate their ability to potentiate radiation-induced DNA damage, cell function, cell proliferation. Exploring the radiation-induced DNA damage by using the alkaline comet assay, αKG-treatment alone was unable to provoke more DNA damage than non-treated control group, but it significantly enhanced DNA damage induced by CTPI2-treatment. Similar results were also observed in octyl-D2HG and octyl-D2HG+αKG treatment groups, implying that CTPI2-induced DNA damage was based on the effect of D-2HG.

Slightly different results were detected by γ-H2AX analysis. Here, αKG-treatment alone stimulated γ-H2AX formation upon IR-treatment and acted as an enhancer for CTPI2's effect. On the contrary, αKG-treatment did not enhance γ-H2AX formation induced by octyl-D2HG-treatment, which indicated that CTPI2 and octyl-D2HG acted differently on DSB, the most lethal damage on DNA (Chowdhury et al., 2005). Although αKG-treatment enhanced the generation of cytoplasmic ROS induced by CTPI2-treatment with or without IR, αKG-treatment alone did not have any significant effect on ROS formation. Consistent results also came from apoptosis, cell death, mitochondrial function and cell proliferation analysis, indicating CTPI2 was the leading player with assistance of αKG to exert its effect on the describes functional read outs upon treatment. On the other hand, the replacement of SLC25A1-inhibition by CTPI2-treatment with octyl-D2HG-treatment were not so consistent in modulating measured cellular function as CTPI2-treatment did. This result underlined the broad multifactorial metabolic reprogramming induced by CTPI2-mediated inhibition of SLC25A1, among those accumulation of D-2HG seems to be one major mechanism affecting cellular function and DNA damage repair induced upon IR. Thus, treatment of cells with octyl-D2HG, still allowing the cell to exchange

citrate turned out to be less lethal and suitable for radiosensitization. Analysing cellular viability/proliferation, αKG-treatment was tending to counteract the proliferation suppression effect induced by octyl-D2HG, suggesting αKG may recapture the binding ability to αKGDD to save the effect of octyl-D2HG. However, again, αKG-treatment was not able to abrogate the inhibition of proliferation induced by CTPI2, hinting to distinct effects of octyl-D2HG application and the complex metabolic reprogramming induced by CTPI2 treatment.

Since both treatments with CTPI2 and octyl-D2HG eliminated the amount of NAD+, NADH, NADP+ and NADPH, these effects were counteracted by adding their precursor NAM with the attempt to examine whether NAM-supplementation would save the effect of CTPI2 and octyl-D2HG on NAD-depletion. Nicotinamide (NAM) is an amide form of vitamin B3 and the precursor of NAD+, an essential co-enzyme of redox reactions for adenosine triphosphate (ATP) production and for other metabolic processes (Fania et al., 2019). In our γ-H2AX analysis, NAM-supplementation alleviated the damaging effect of CTPI2 and CTPI2+αKG-treatments. This is in accordance with NAM's effect on genomic stability, which was supported by ATP-assistant DNA repair enzymes (Fania *et al.*, 2019). Relieving impact of NAM on CTPI2 or CTPI2+αKG induced cytoplasmic ROS production, apoptosis-, cell death-levels, mitochondrial function and cell proliferation was observed, implying that decreasing amount of NAD+, NADH, NADP+ and NADPH may play important role upon inhibition of SLC25A1 in NCI-H460 cancer cells. In contrast, no consistent conclusion can be drawn from NAM-supplementation experiments in combination with octyl-D2HG treatment. These observations corroborate the conclusion on distinct mechanisms induced by octyl-D2HG treatment compared to CTPI2-treatment. Furthermore, NAM was employed in addition to CTPI2 or octyl-D2HG to check if NAM could save the oxidative state induced by the latter two treatments. Here, NAM supplementation only rescued CTPI2 treatment-induced NAD depletion significantly. Considering ROS generation, apoptosis induction, DNA damage, mitochondrial dysfunction mediated by CTPI2, and its effect can be saved by NAM, implying that it was the ratio, which led to oxidative state, that counts, rather than the exact amount of NAD^+ and NADH.

4.4 Interference with KDMs

Next, a potential involvement of KDM inhibition in the proposed mechanism of action of disturbance of DNA repair by D-2HG accumulation was examined by comparing the effects of KDMs-inhibition with a pan KDM-inhibitor JIB-04 and CTPI2 treatment. JIB-04 inhibits the demethylase activity of Jumonji enzymes, one of the major KDM sub-families in cells, without affecting αKG-dependent prolyl hydroxylases and TET enzymes or other chromatin-modifying enzymes such as histone deacetylases (Cascella et al., 2017; Wang *et al.*, 2013). Treatment with JIB-04 increased radiation-induced γ-H2AX accumulation at 6h after IR. These results further consolidate JIB-04's ability to amplify or impair the removal of radiation-induced γ-H2AX and thus potentially impair the repair of radiation-induced DNA damage (Parrish et al., 2018). Furthermore, the results provide first evidence on a combinatorial effect of KDM-inhibition by JIB-04 and additional αKG-treatment for radiosensitization. Corresponding to the observation on the CTPI2-induced cytoplasmic ROS stimulation, DHE staining was also employed to detect the increasing cytoplasmic ROS generation induced by JIB-04. According to previous studies, ROS generation was accompanied by Wnt/β-catenin pathway inhibition, which could be activated by ROS scavenger, suggesting that Wnt/β-catenin pathway may play an important role in ROS generation (Wang et al., 2021). Intriguingly, JIB-04-treatment was found to be negatively related with Wnt/β-catenin pathway (Kim et al., 2018). It was tempting to speculate whether JIB-04 treatment-induced ROS generation was mediated by Wnt/β-catenin pathway, which would be worthwhile for further exploration. Inhibition of KDMs by JIB-04-treatment was shown to induce apoptosis via activation of p53/Bcl-2 caspase pathway (Liao et al., 2018). In the present study, a slight increase of apoptosis level upon JIB-04 treatment was observed without IR, nonetheless, the level of apoptosis increased sharply with αKG supplementation, indicating that αKG may support the activation of p53/Bcl-2 caspase pathway (Figure 12c). JIB-04-treatment had been suggested for application in clinical trial since it altered transcriptional growth programs in cancer but not in normal cells, resulting in cancer-specific cell death (Parrish *et al.*, 2018; Wang *et al.*, 2013). In compliance with this reported result, JIB-04 treatment increased the level of cell death and reduced cell proliferation, with or without IR in the present study. Of note, the antineoplastic effects of JIB-04-treatment recapitulated the phenotype induced by CTPI2-treatment and was significantly enhanced by αKG

supplementation which is consistent with the findings obtained with CTPI2 treatment (Figure 12d, e).

4.5 *In vivo* validation of CTPI2 induced HR-ness (CAM model)

Finally, the impact of observed disturbance of cell function and metabolism following CTPI2-treatment *in vitro* was tested for its effects on tumor formation and growth *in vivo*. Herein, a CAM model was established and used to evaluate the antitumor capacity of SLC25A1i *in vivo*. In accordance with the *in vitro* effects, exposure to CTPI2-treatment led to statistically smaller tumor size compared to untreated control tumors. The potential connection between D2HG accumulation induced by CTPI2-treatment and its described negative effects on HRR pathway motivated us to test inhibition of SLC25A1 with EJ-pathway inhibition by inhibiting PARP and investigate the influence of the combination treatment on tumor growth upon IR. Remarkably, PARPi alone didn't affect tumor growth under the circumstances of IR. However, decreasing the functionality of HRR (HR-ness phenotype) by SLC25A1 inhibition significantly reduced tumor growth in combination with PARPi by PJ34, thus blocking the major DNA damage repairing pathways upon IR-treatment. The obtained *in vivo* result recapitulated the observed *in vitro* effects of CTPI2 treatment, validating that disturbance of cell function, interference with DNA damage repair, and mitochondrial function results in tumor suppression in combination with IR.

In summary, the present study extends previous observations which indicating SLC25A1 inhibition is suited to sensitize cancer cells to IR (Hlouschek *et al.*, 2018a). The obtained results demonstrated important cellular responses altered upon SLC25A1 inhibition by CTPI2 exposure. D-2HG level increased and stayed upregulated when cancer cells were treated with pharmacological inhibition of SLC25A1. Both CTPI2 and cell permeable D-2HG induced ROS production, shifted cellular balance to oxidative state of NAD^+/NADH, $NADP^+$/NADPH co-enzymes and increased dependence on NAD and NADP. Alteration of these processes induced by SLC25A1-inhibition by using CTPI2 hints to complex multimodal metabolic reprogramming of cellular processes important for survival of radiation-induced damage. In detail, CTPI2 or cell permeable D-2HG brought about more DNA damage and delayed DNA repair. In addition, mitochondrial function was also

impaired by CTPI2 and octyl-D2HG treatment. In accordance with cellular function destruction, cell proliferation could be inhibited by CTPI2 both *in vitro* and *in vivo*. αKG supplementation revealed that CTPI2's effect on D2HG production, ROS generation, apoptosis and cell death induction, mitochondrial dysfunction and DNA damage is potentiated by αKG, but can be counteracted by NAM, except for D-2HG production. Furthermore, direct targeting of KDMs by JIB-04 application was mimicking the effect of CTPI2 on DNA damage and cell function aspects (Figure 13).

These results corroborate that the effects of CTPI2-mediated inhibition of SLC25A1 are, at least partially, explained by D-2HG accumulation and its inhibitory effects on KDMs as well as the additional disturbance of NAD^+/NADH ratio affecting the dependence of cancer cells on NAD. Further efforts are necessary to unravel the complete picture of CTPI2-induced metabolic reprogramming and D-2HG production, to confirm the relationship between SLC25A1 and the oncometabolite D-2HG, and to identify potential other D-2HG inducing targets suitable for tumor radiosensitization.

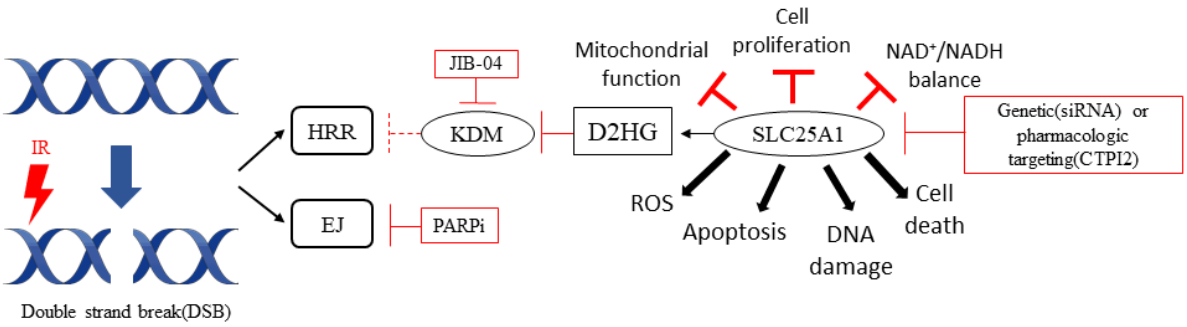

Figure 13: Schematic representation of the suggested mechanisms of the actions of CTPI2 and IR on cancer cell metabolism and DNA damage response.

Pharmacological inhibition of SLC25A1 induced alterations of cellular biological activities, including suppressed mitochondrial function, reduced cell proliferation, disturbance of NAD+/NADH balance, ROS generation, as well as induction of DNA damage, apoptosis, and cell death. CTPI2 induced D-2HG overproduction, which might lead to KDM inhibition and resulting interference with HRR. Metabolic disturbance of HRR renders cancer cells more vulnerable to end-joining (EJ) pathway inhibitors, such as PARPi.

5 Summary

5.1 English summary

Radiotherapy (RT) alleviates the tumor burden for cancer patients. However, radioresistance is one of the major obstacles for efficient RT, one of the reasons is cancer metabolic reprogramming. Metabolic reprogramming leads to production of cancer-associated metabolites, called “oncometabolites”, one of which is 2-hyroxyglutarate (2-HG). Previous work of our group has shown that inhibition of the citrate transport protein (SLC25A1) leads to overproduction of D-2HG, one enantiomer of 2-HG, and disturbance of the DNA damage response (DDR). In this thesis, inhibition of SLC25A1 with CTPI2 resulted in sustained D-2HG accumulation. CTPI2 treatment, as well as cell permeable D-2HG (octyl-D2HG) treatment, potentiated radiation-induced DNA damage. Furthermore, CTPI2 and octyl-D2HG treatment both provoked cytoplasmic or mitochondrial ROS generation, apoptosis induction, cell death, mitochondrial dysfunction, and cell proliferation/viability inhibition, as well as increased radiosensitivity. Mechanistically, CTPI2 or octyl-D2HG treatment induced an oxidative cellular state that affected nicotinamide adenine dinucleotide (NAD^+/NADH) or nicotinamide adenine dinucleotide phosphate ($NADP^+$/NADPH) ratios. CTPI2-treatment of NCI-H460 tumors on chicken chorioallantoic membrane (CAM) model *in vivo* led to a tumor growth inhibition, which was potentiated by poly (ADP-ribose)-polymerase inhibition (PARPi) in combination with IR. Interestingly, α-ketoglutarate (αKG) supplementation potentiated CTPI2’s effect on D-2HG overproduction, DNA damage induction, and disturbance of cellular function, which was counteracted by supplementation of nicotinamide (NAM). Additionally, histone-lysine demethylase (KDM) inhibition by JIB-04 recapitulated CTPI2’s effect on γH2A.X foci formation and on cellular function, and was also potentiated by supplementation with αKG. In conclusion, SLC25A1 inhibition might be suited for pharmacologic induction of synthetic lethality in combination with clinically relevant DSB repair inhibitors in cancer cells.

5.2 Deutsche Zusammenfassung

Die Strahlentherapie (RT) lindert die Tumorlast bei Krebspatienten. Allerdings ist die Strahlenresistenz eines der Haupthindernisse für eine effiziente RT, einer der Gründe dafür ist die metabolische Umprogrammierung von Krebs. Metabolische Umprogrammierung führt zur Produktion von krebsassoziierten Metaboliten, den so genannten "Oncometaboliten", zu denen auch 2-Hyroxyglutarat (2-HG) gehört. Frühere Arbeiten unserer Gruppe haben gezeigt, dass die Hemmung des Citrat-Transportproteins (SLC25A1) zu einer Überproduktion von D-2HG, einem Enantiomer von 2-HG, und einer Störung der DNA-Schadensantwort (DDR) führt. In dieser Arbeit führte die Hemmung von SLC25A1 mit CTPI2 zu einer anhaltenden D-2HG-Akkumulation. Die CTPI2-Behandlung sowie die Behandlung mit zelldurchlässigem D-2HG (Octyl-D2HG) verstärkten die strahleninduzierten DNA-Schäden. Darüber hinaus führte sowohl die Behandlung mit CTPI2 als auch mit Octyl-D2HG zu zytoplasmatischer oder mitochondrialer ROS-Bildung, Apoptose-Induktion, Zelltod, mitochondrialer Dysfunktion und Hemmung der Zellproliferation sowie zu erhöhter Radiosensitivität. Mechanistisch gesehen induzierte die Behandlung mit CTPI2 oder Octyl-D2HG einen oxidativen Zellzustand, der das Verhältnis von Nicotinamid-Adenin-Dinukleotid (NAD+/NADH) oder Nicotinamid-Adenin-Dinukleotid-Phosphat (NADP+/NADPH) beeinflusste. Die CTPI2-Behandlung von NCI-H460-Tumoren im Hühner-Chorioallantoismembran (CAM)-Modell *in vivo* führte zu einer Hemmung des Tumorwachstums, die durch die Hemmung der Poly (ADP-Ribose)-Polymerase (PARPi) in Kombination mit IR verstärkt wurde. Interessanterweise verstärkte die Supplementierung von α-Ketoglutarat (αKG) die Wirkung von CTPI2 auf die D-2HG-Überproduktion, die Induktion von DNA-Schäden und die Störung der gemessenen Zellfunktionen, was durch die Supplementierung von Nicotinamid (NAM) ausgeglichen wurde. Zusätzlich rekapitulierte die Hemmung der Histon-Lysin-Demethylase (KDM) durch JIB-04 die Wirkung von CTPI2 auf die Bildung von γH2A.X-Foci und auf die Zellfunktionen und wurde durch eine Supplementierung mit αKG ebenfalls verstärkt. Zusammenfassend lässt sich sagen, dass die Hemmung von SLC25A1 für die pharmakologische Induktion von synthetischer Letalität in Kombination mit klinisch relevanten DSB-Reparaturinhibitoren in Krebszellen geeignet sein könnte.

6 References

1 Abshire, D., and Lang, M.K. (2018). The Evolution of Radiation Therapy in Treating Cancer. Semin Oncol Nurs *34*, 151-157. 10.1016/j.soncn.2018.03.006.

2 Belenky, P., Bogan, K.L., and Brenner, C. (2007). NAD+ metabolism in health and disease. Trends Biochem Sci *32*, 12-19. 10.1016/j.tibs.2006.11.006.

3 Brahimi-Horn, M.C., Chiche, J., and Pouyssegur, J. (2007). Hypoxia and cancer. J Mol Med (Berl) *85*, 1301-1307. 10.1007/s00109-007-0281-3.

4 Bristow, R.G., and Hill, R.P. (2008). Hypoxia and metabolism. Hypoxia, DNA repair and genetic instability. Nat Rev Cancer *8*, 180-192. 10.1038/nrc2344.

5 Buque, A., Bloy, N., Kroemer, G., and Galluzzi, L. (2021). Possible mechanisms of cancer prevention by nicotinamide. Br J Pharmacol *178*, 2034-2040. 10.1111/bph.15096.

6 Canto, C., Menzies, K.J., and Auwerx, J. (2015). NAD(+) Metabolism and the Control of Energy Homeostasis: A Balancing Act between Mitochondria and the Nucleus. Cell Metab *22*, 31-53. 10.1016/j.cmet.2015.05.023.

7 Cantor, J.R., and Sabatini, D.M. (2012). Cancer cell metabolism: one hallmark, many faces. Cancer Discov *2*, 881-898. 10.1158/2159-8290.CD-12-0345.

8 Cascella, B., Lee, S.G., Singh, S., Jez, J.M., and Mirica, L.M. (2017). The small molecule JIB-04 disrupts O2 binding in the Fe-dependent histone demethylase KDM4A/JMJD2A. Chem Commun (Camb) *53*, 2174-2177. 10.1039/c6cc09882g.

9 Catalina-Rodriguez, O., Kolukula, V.K., York Tomita, A.P., Palmieri, F., Wellstein, A., Byers, S., Giaccia, A.J., Glasgow, E., Albanese, C., and Avantaggiati, M.L. (2012). The mitochondrial citrate transporter, CIC, is essential for mitochondrial homeostasis. Oncotarget *3*, 1220.

10 Chowdhury, D., Keogh, M.C., Ishii, H., Peterson, C.L., Buratowski, S., and Lieberman, J. (2005). gamma-H2AX dephosphorylation by protein phosphatase 2A facilitates DNA double-strand break repair. Mol Cell *20*, 801-809. 10.1016/j.molcel.2005.10.003.

11 Cohen, I., Staretz-Chacham, O., Wormser, O., Perez, Y., Saada, A., Kadir, R., and Birk, O.S. (2018). A novel homozygous SLC25A1 mutation with

impaired mitochondrial complex V: Possible phenotypic expansion. Am J Med Genet A *176*, 330-336. 10.1002/ajmg.a.38574.

12 DeBerardinis, R.J., and Chandel, N.S. (2016). Fundamentals of cancer metabolism. Science advances *2*, e1600200.

13 DeBerardinis, R.J., Mancuso, A., Daikhin, E., Nissim, I., Yudkoff, M., Wehrli, S., and Thompson, C.B. (2007). Beyond aerobic glycolysis: transformed cells can engage in glutamine metabolism that exceeds the requirement for protein and nucleotide synthesis. Proceedings of the National Academy of Sciences *104*, 19345-19350.

14 Fania, L., Mazzanti, C., Campione, E., Candi, E., Abeni, D., and Dellambra, E. (2019). Role of Nicotinamide in Genomic Stability and Skin Cancer Chemoprevention. Int J Mol Sci *20*. 10.3390/ijms20235946.

15 Flavin, R., Peluso, S., Nguyen, P.L., and Loda, M. (2010). Fatty acid synthase as a potential therapeutic target in cancer. Future oncology *6*, 551-562.

16 Floberg, J.M., and Schwarz, J.K. (2019). Manipulation of Glucose and Hydroperoxide Metabolism to Improve Radiation Response. Semin Radiat Oncol *29*, 33-41. 10.1016/j.semradonc.2018.10.007.

17 Frey, T.G., and Mannella, C.A. (2000). The internal structure of mitochondria. Trends in biochemical sciences *25*, 319-324.

18 Frezza, C. (2014). The role of mitochondria in the oncogenic signal transduction. Int J Biochem Cell Biol *48*, 11-17. 10.1016/j.biocel.2013.12.013.

19 Gao, P., Zhang, H., Dinavahi, R., Li, F., Xiang, Y., Raman, V., Bhujwalla, Z.M., Felsher, D.W., Cheng, L., Pevsner, J., Lee, L.A., Semenza, G.L., and Dang, C.V. (2007). HIF-dependent antitumorigenic effect of antioxidants in vivo. Cancer Cell *12*, 230-238. 10.1016/j.ccr.2007.08.004.

20 Gaude, E., and Frezza, C. (2014). Defects in mitochondrial metabolism and cancer. Cancer & metabolism *2*, 1-9.

21 Gaude, E., and Frezza, C. (2016). Tissue-specific and convergent metabolic transformation of cancer correlates with metastatic potential and patient survival. Nat Commun *7*, 13041. 10.1038/ncomms13041.

22 Giannoni, E., Buricchi, F., Raugei, G., Ramponi, G., and Chiarugi, P. (2005). Intracellular reactive oxygen species activate Src tyrosine kinase during cell

adhesion and anchorage-dependent cell growth. Mol Cell Biol *25*, 6391-6403. 10.1128/MCB.25.15.6391-6403.2005.

23 Hinshaw, D.C., and Shevde, L.A. (2019). The Tumor Microenvironment Innately Modulates Cancer Progression. Cancer Res *79*, 4557-4566. 10.1158/0008-5472.CAN-18-3962.

24 Hlouschek, J., Hansel, C., Jendrossek, V., and Matschke, J. (2018a). The Mitochondrial Citrate Carrier (SLC25A1) Sustains Redox Homeostasis and Mitochondrial Metabolism Supporting Radioresistance of Cancer Cells With Tolerance to Cycling Severe Hypoxia. Front Oncol *8*, 170. 10.3389/fonc.2018.00170.

25 Hlouschek, J., Ritter, V., Wirsdorfer, F., Klein, D., Jendrossek, V., and Matschke, J. (2018b). Targeting SLC25A10 alleviates improved antioxidant capacity and associated radioresistance of cancer cells induced by chronic-cycling hypoxia. Cancer Lett *439*, 24-38. 10.1016/j.canlet.2018.09.002.

26 Icard, P., Poulain, L., and Lincet, H. (2012). Understanding the central role of citrate in the metabolism of cancer cells. Biochim Biophys Acta *1825*, 111-116. 10.1016/j.bbcan.2011.10.007.

27 Intlekofer, A.M., Dematteo, R.G., Venneti, S., Finley, L.W., Lu, C., Judkins, A.R., Rustenburg, A.S., Grinaway, P.B., Chodera, J.D., Cross, J.R., and Thompson, C.B. (2015). Hypoxia Induces Production of L-2-Hydroxyglutarate. Cell Metab *22*, 304-311. 10.1016/j.cmet.2015.06.023.

28 Intlekofer, A.M., Wang, B., Liu, H., Shah, H., Carmona-Fontaine, C., Rustenburg, A.S., Salah, S., Gunner, M.R., Chodera, J.D., Cross, J.R., and Thompson, C.B. (2017). L-2-Hydroxyglutarate production arises from noncanonical enzyme function at acidic pH. Nat Chem Biol *13*, 494-500. 10.1038/nchembio.2307.

29 Jezek, J., Cooper, K.F., and Strich, R. (2018). Reactive Oxygen Species and Mitochondrial Dynamics: The Yin and Yang of Mitochondrial Dysfunction and Cancer Progression. Antioxidants (Basel) *7*. 10.3390/antiox7010013.

30 Johnson, T.I., Costa, A.S.H., Ferguson, A.N., and Frezza, C. (2018). Fumarate hydratase loss promotes mitotic entry in the presence of DNA damage after ionising radiation. Cell Death Dis *9*, 913. 10.1038/s41419-018-0912-3.

31 Kaelin Jr, W.G., and McKnight, S.L. (2013). Influence of metabolism on epigenetics and disease. Cell *153*, 56-69.

32 Kauffman, M.E., Kauffman, M.K., Traore, K., Zhu, H., Trush, M.A., Jia, Z., and Li, Y.R. (2016). MitoSOX-Based Flow Cytometry for Detecting Mitochondrial ROS. React Oxyg Species (Apex) *2*, 361-370. 10.20455/ros.2016.865.

33 Khanna, K.K., and Jackson, S.P. (2001). DNA double-strand breaks: signaling, repair and the cancer connection. Nature genetics *27*, 247-254.

34 Kim, M.S., Cho, H.I., Yoon, H.J., Ahn, Y.H., Park, E.J., Jin, Y.H., and Jang, Y.K. (2018). JIB-04, A Small Molecule Histone Demethylase Inhibitor, Selectively Targets Colorectal Cancer Stem Cells by Inhibiting the Wnt/beta-Catenin Signaling Pathway. Sci Rep *8*, 6611. 10.1038/s41598-018-24903-0.

35 King, A., Selak, M.A., and Gottlieb, E. (2006). Succinate dehydrogenase and fumarate hydratase: linking mitochondrial dysfunction and cancer. Oncogene *25*, 4675-4682. 10.1038/sj.onc.1209594.

36 Kirkman, H.N., and Gaetani, G.F. (1984). Catalase: a tetrameric enzyme with four tightly bound molecules of NADPH. Proceedings of the national academy of sciences *81*, 4343-4347.

37 Kirsch, D.G., Diehn, M., Kesarwala, A.H., Maity, A., Morgan, M.A., Schwarz, J.K., Bristow, R., Demaria, S., Eke, I., Griffin, R.J., Haas-Kogan, D., Higgins, G.S., Kimmelman, A.C., Kimple, R.J., Lombaert, I.M., Ma, L., Marples, B., Pajonk, F., Park, C.C., Schaue, D., Tran, P.T., Willers, H., Wouters, B.G., and Bernhard, E.J. (2018). The Future of Radiobiology. J Natl Cancer Inst *110*, 329-340. 10.1093/jnci/djx231.

38 Kolukula, V.K., Sahu, G., Wellstein, A., Rodriguez, O.C., Preet, A., Iacobazzi, V., D'Orazi, G., Albanese, C., Palmieri, F., and Avantaggiati, M.L. (2014). SLC25A1, or CIC, is a novel transcriptional target of mutant p53 and a negative tumor prognostic marker. Oncotarget *5*, 1212.

39 Legendre, F., MacLean, A., Appanna, V.P., and Appanna, V.D. (2020). Biochemical pathways to alpha-ketoglutarate, a multi-faceted metabolite. World J Microbiol Biotechnol *36*, 123. 10.1007/s11274-020-02900-8.

40 Li, F., Zhou, K., Gao, L., Zhang, B., Li, W., Yan, W., Song, X., Yu, H., Wang, S., Yu, N., and Jiang, Q. (2016). Radiation induces the generation of cancer stem cells: A novel mechanism for cancer radioresistance. Oncol Lett *12*, 3059-3065. 10.3892/ol.2016.5124.

41 Li, X., Zhuang, X., and Qiao, T. (2019). Role of ferroptosis in the process of acute radiation-induced lung injury in mice. Biochem Biophys Res Commun *519*, 240-245. 10.1016/j.bbrc.2019.08.165.

42 Li, Z., Peng, H., Qin, L., Qi, J., Zuo, X., Liu, J.Y., and Zhang, J.T. (2013). Determinants of 14-3-3sigma protein dimerization and function in drug and radiation resistance. J Biol Chem *288*, 31447-31457. 10.1074/jbc.M113.467753.

43 Liao, W., Liu, J., Liu, B., Huang, X., Yin, Y., Cai, Li, M., and Zhu, R. (2018). JIB04 induces cell apoptosis via activation of the p53/Bcl2/caspase pathway in MHCC97H and HepG2 cells. Oncol Rep *40*, 3812-3820. 10.3892/or.2018.6737.

44 Locasale, J.W., Grassian, A.R., Melman, T., Lyssiotis, C.A., Mattaini, K.R., Bass, A.J., Heffron, G., Metallo, C.M., Muranen, T., Sharfi, H., Sasaki, A.T., Anastasiou, D., Mullarky, E., Vokes, N.I., Sasaki, M., Beroukhim, R., Stephanopoulos, G., Ligon, A.H., Meyerson, M., Richardson, A.L., Chin, L., Wagner, G., Asara, J.M., Brugge, J.S., Cantley, L.C., and Vander Heiden, M.G. (2011). Phosphoglycerate dehydrogenase diverts glycolytic flux and contributes to oncogenesis. Nat Genet *43*, 869-874. 10.1038/ng.890.

45 Martinez-Carreres, L., Nasrallah, A., and Fajas, L. (2017). Cancer: Linking Powerhouses to Suicidal Bags. Front Oncol *7*, 204. 10.3389/fonc.2017.00204.

46 Martinez-Outschoorn, U.E., Peiris-Pages, M., Pestell, R.G., Sotgia, F., and Lisanti, M.P. (2017). Cancer metabolism: a therapeutic perspective. Nat Rev Clin Oncol *14*, 11-31. 10.1038/nrclinonc.2016.60.

47 Matschke, J., Larafa, S., and Jendrossek, V. (2021). Metabolic reprograming of antioxidant defense: a precision medicine perspective for radiotherapy of lung cancer? Biochemical Society Transactions.

48 Matschke, J., Riffkin, H., Klein, D., Handrick, R., Ludemann, L., Metzen, E., Shlomi, T., Stuschke, M., and Jendrossek, V. (2016a). Targeted Inhibition of

Glutamine-Dependent Glutathione Metabolism Overcomes Death Resistance Induced by Chronic Cycling Hypoxia. Antioxid Redox Signal *25*, 89-107. 10.1089/ars.2015.6589.

49 Matschke, J., Wiebeck, E., Hurst, S., Rudner, J., and Jendrossek, V. (2016b). Role of SGK1 for fatty acid uptake, cell survival and radioresistance of NCI-H460 lung cancer cells exposed to acute or chronic cycling severe hypoxia. Radiat Oncol *11*, 75. 10.1186/s13014-016-0647-1.

50 McNeill, K.A. (2016). Epidemiology of Brain Tumors. Neurol Clin *34*, 981-998. 10.1016/j.ncl.2016.06.014.

51 Mizushima, N., and Levine, B. (2020). Autophagy in Human Diseases. N Engl J Med *383*, 1564-1576. 10.1056/NEJMra2022774.

52 Mladenov, E., and Iliakis, G. (2011). Induction and repair of DNA double strand breaks: the increasing spectrum of non-homologous end joining pathways. Mutat Res *711*, 61-72. 10.1016/j.mrfmmm.2011.02.005.

53 Morciano, P., Carrisi, C., Capobianco, L., Mannini, L., Burgio, G., Cestra, G., De Benedetto, G.E., Corona, D.F., Musio, A., and Cenci, G. (2009). A conserved role for the mitochondrial citrate transporter Sea/SLC25A1 in the maintenance of chromosome integrity. Hum Mol Genet *18*, 4180-4188. 10.1093/hmg/ddp370.

54 Mullen, A.R., Hu, Z., Shi, X., Jiang, L., Boroughs, L.K., Kovacs, Z., Boriack, R., Rakheja, D., Sullivan, L.B., Linehan, W.M., Chandel, N.S., and DeBerardinis, R.J. (2014). Oxidation of alpha-ketoglutarate is required for reductive carboxylation in cancer cells with mitochondrial defects. Cell Rep *7*, 1679-1690. 10.1016/j.celrep.2014.04.037.

55 Mullen, A.R., Wheaton, W.W., Jin, E.S., Chen, P.H., Sullivan, L.B., Cheng, T., Yang, Y., Linehan, W.M., Chandel, N.S., and DeBerardinis, R.J. (2011). Reductive carboxylation supports growth in tumour cells with defective mitochondria. Nature *481*, 385-388. 10.1038/nature10642.

56 Nanya, M., Sato, M., Tanimoto, K., Tozuka, M., Mizutani, S., and Takagi, M. (2015). Dysregulation of the DNA Damage Response and KMT2A Rearrangement in Fetal Liver Hematopoietic Cells. PLoS One *10*, e0144540. 10.1371/journal.pone.0144540.

57 Nicoletti, I., Migliorati, G., Pagliacci, M., Grignani, F., and Riccardi, C. (1991). A rapid and simple method for measuring thymocyte apoptosis by propidium iodide staining and flow cytometry. Journal of immunological methods *139*, 271-279.

58 Oermann, E.K., Wu, J., Guan, K.-L., and Xiong, Y. (2012). Alterations of metabolic genes and metabolites in cancer. In 4. (Elsevier), pp. 370-380.

59 Owen, O.E., Kalhan, S.C., and Hanson, R.W. (2002). The key role of anaplerosis and cataplerosis for citric acid cycle function. J Biol Chem *277*, 30409-30412. 10.1074/jbc.R200006200.

60 Park, S.Y., Le, C.T., Sung, K.Y., Choi, D.H., and Cho, E.H. (2018). Succinate induces hepatic fibrogenesis by promoting activation, proliferation, and migration, and inhibiting apoptosis of hepatic stellate cells. Biochem Biophys Res Commun *496*, 673-678. 10.1016/j.bbrc.2018.01.106.

61 Parrish, J.K., McCann, T.S., Sechler, M., Sobral, L.M., Ren, W., Jones, K.L., Tan, A.C., and Jedlicka, P. (2018). The Jumonji-domain histone demethylase inhibitor JIB-04 deregulates oncogenic programs and increases DNA damage in Ewing Sarcoma, resulting in impaired cell proliferation and survival, and reduced tumor growth. Oncotarget *9*, 33110.

62 Pavlova, N.N., and Thompson, C.B. (2016). The Emerging Hallmarks of Cancer Metabolism. Cell Metab *23*, 27-47. 10.1016/j.cmet.2015.12.006.

63 Perland, E., and Fredriksson, R. (2017). Classification Systems of Secondary Active Transporters. Trends Pharmacol Sci *38*, 305-315. 10.1016/j.tips.2016.11.008.

64 Prasun, P., Young, S., Salomons, G., Werneke, A., Jiang, Y.H., Struys, E., Paige, M., Avantaggiati, M.L., and McDonald, M. (2015). Expanding the Clinical Spectrum of Mitochondrial Citrate Carrier (SLC25A1) Deficiency: Facial Dysmorphism in Siblings with Epileptic Encephalopathy and Combined D,L-2-Hydroxyglutaric Aciduria. JIMD Rep *19*, 111-115. 10.1007/8904_2014_378.

65 Pu, X., Wang, Z., and Klaunig, J.E. (2015). Alkaline Comet Assay for Assessing DNA Damage in Individual Cells. Curr Protoc Toxicol *65*, 3 12 11-13 12 11. 10.1002/0471140856.tx0312s65.

66 Reinfeld, B.I., Madden, M.Z., Wolf, M.M., Chytil, A., Bader, J.E., Patterson, A.R., Sugiura, A., Cohen, A.S., Ali, A., Do, B.T., Muir, A., Lewis, C.A., Hongo, R.A., Young, K.L., Brown, R.E., Todd, V.M., Huffstater, T., Abraham, A., O'Neil, R.T., Wilson, M.H., Xin, F., Tantawy, M.N., Merryman, W.D., Johnson, R.W., Williams, C.S., Mason, E.F., Mason, F.M., Beckermann, K.E., Vander Heiden, M.G., Manning, H.C., Rathmell, J.C., and Rathmell, W.K. (2021). Cell-programmed nutrient partitioning in the tumour microenvironment. Nature *593*, 282-288. 10.1038/s41586-021-03442-1.

67 Ribatti, D. (2016). The chick embryo chorioallantoic membrane (CAM). A multifaceted experimental model. Mech Dev *141*, 70-77. 10.1016/j.mod.2016.05.003.

68 Roos, W.P., Thomas, A.D., and Kaina, B. (2016). DNA damage and the balance between survival and death in cancer biology. Nature Reviews Cancer *16*, 20-33.

69 Ruprecht, J.J., and Kunji, E.R.S. (2020). The SLC25 Mitochondrial Carrier Family: Structure and Mechanism. Trends Biochem Sci *45*, 244-258. 10.1016/j.tibs.2019.11.001.

70 Sakaue, H., and Endo, T. (2019). Regulation of the protein entry gate assembly by mitochondrial porin. Curr Genet *65*, 1161-1163. 10.1007/s00294-019-00979-7.

71 Schmidt, C., Sciacovelli, M., and Frezza, C. (2020). Fumarate hydratase in cancer: A multifaceted tumour suppressor. Semin Cell Dev Biol *98*, 15-25. 10.1016/j.semcdb.2019.05.002.

72 Shadel, G.S., and Horvath, T.L. (2015). Mitochondrial ROS signaling in organismal homeostasis. Cell *163*, 560-569. 10.1016/j.cell.2015.10.001.

73 Sherratt, H. (1991). Mitochondria: structure and function. Revue neurologique *147*, 417-430.

74 Sitthideatphaiboon, P., Galan-Cobo, A., Negrao, M.V., Qu, X., Poteete, A., Zhang, F., Liu, D.D., Lewis, W.E., Kemp, H.N., and Lewis, J. (2021). STK11/LKB1 mutations in NSCLC are associated with KEAP1/NRF2-dependent radiotherapy resistance targetable by glutaminase inhibition. Clinical Cancer Research *27*, 1720-1733.

75 Spitz, D.R., Azzam, E.I., Li, J.J., and Gius, D. (2004). Metabolic oxidation/reduction reactions and cellular responses to ionizing radiation: a unifying concept in stress response biology. Cancer and Metastasis Reviews *23*, 311-322.

76 Staaf, E., Brehwens, K., Haghdoost, S., Czub, J., and Wojcik, A. (2012). Gamma-H2AX foci in cells exposed to a mixed beam of X-rays and alpha particles. Genome integrity *3*, 1-13.

77 Sulkowski, P.L., Corso, C.D., Robinson, N.D., Scanlon, S.E., Purshouse, K.R., Bai, H., Liu, Y., Sundaram, R.K., Hegan, D.C., and Fons, N.R. (2017). 2-Hydroxyglutarate produced by neomorphic IDH mutations suppresses homologous recombination and induces PARP inhibitor sensitivity. Science translational medicine *9*.

78 Sulkowski, P.L., Oeck, S., Dow, J., Economos, N.G., Mirfakhraie, L., Liu, Y., Noronha, K., Bao, X., Li, J., Shuch, B.M., King, M.C., Bindra, R.S., and Glazer, P.M. (2020). Oncometabolites suppress DNA repair by disrupting local chromatin signalling. Nature *582*, 586-591. 10.1038/s41586-020-2363-0.

79 Sung, H., Ferlay, J., Siegel, R.L., Laversanne, M., Soerjomataram, I., Jemal, A., and Bray, F. (2021). Global Cancer Statistics 2020: GLOBOCAN Estimates of Incidence and Mortality Worldwide for 36 Cancers in 185 Countries. CA Cancer J Clin *71*, 209-249. 10.3322/caac.21660.

80 Takahashi, A., Ohtani, N., Yamakoshi, K., Iida, S., Tahara, H., Nakayama, K., Nakayama, K.I., Ide, T., Saya, H., and Hara, E. (2006). Mitogenic signalling and the p16INK4a-Rb pathway cooperate to enforce irreversible cellular senescence. Nat Cell Biol *8*, 1291-1297. 10.1038/ncb1491.

81 Tamulevicius, P., Wang, M., and Iliakis, G. (2007). Homology-directed repair is required for the development of radioresistance during S phase: interplay between double-strand break repair and checkpoint response. Radiation research *167*, 1-11.

82 Tan, M., Mosaoa, R., Graham, G.T., Kasprzyk-Pawelec, A., Gadre, S., Parasido, E., Catalina-Rodriguez, O., Foley, P., Giaccone, G., Cheema, A., Kallakury, B., Albanese, C., Yi, C., and Avantaggiati, M.L. (2020). Inhibition

of the mitochondrial citrate carrier, Slc25a1, reverts steatosis, glucose intolerance, and inflammation in preclinical models of NAFLD/NASH. Cell Death Differ *27*, 2143-2157. 10.1038/s41418-020-0491-6.

83 Tominaga, H., Kodama, S., Matsuda, N., Suzuki, K., and Watanabe, M. (2004). Involvement of reactive oxygen species (ROS) in the induction of genetic instability by radiation. Journal of radiation research *45*, 181-188.

84 Tseng, P.L., Wu, W.H., Hu, T.H., Chen, C.W., Cheng, H.C., Li, C.F., Tsai, W.H., Tsai, H.J., Hsieh, M.C., Chuang, J.H., and Chang, W.T. (2018). Decreased succinate dehydrogenase B in human hepatocellular carcinoma accelerates tumor malignancy by inducing the Warburg effect. Sci Rep *8*, 3081. 10.1038/s41598-018-21361-6.

85 Van Vranken, J.G., Na, U., Winge, D.R., and Rutter, J. (2015). Protein-mediated assembly of succinate dehydrogenase and its cofactors. Crit Rev Biochem Mol Biol *50*, 168-180. 10.3109/10409238.2014.990556.

86 Viallard, C., and Larrivee, B. (2017). Tumor angiogenesis and vascular normalization: alternative therapeutic targets. Angiogenesis *20*, 409-426. 10.1007/s10456-017-9562-9.

87 Wang, L., Chang, J., Varghese, D., Dellinger, M., Kumar, S., Best, A.M., Ruiz, J., Bruick, R., Pena-Llopis, S., Xu, J., Babinski, D.J., Frantz, D.E., Brekken, R.A., Quinn, A.M., Simeonov, A., Easmon, J., and Martinez, E.D. (2013). A small molecule modulates Jumonji histone demethylase activity and selectively inhibits cancer growth. Nat Commun *4*, 2035. 10.1038/ncomms3035.

88 Wang, Q., and Zou, M.H. (2018). Measurement of Reactive Oxygen Species (ROS) and Mitochondrial ROS in AMPK Knockout Mice Blood Vessels. Methods Mol Biol *1732*, 507-517. 10.1007/978-1-4939-7598-3_32.

89 Wang, Y.N., Jia, T.T., Feng, Y., Liu, S.Y., Zhang, W.J., Zhang, D.J., and Xu, X. (2021). Hyperlipidemia Impairs Osseointegration via the ROS/Wnt/beta-Catenin Pathway. J Dent Res *100*, 658-665. 10.1177/0022034520983245.

90 Warburg, O. (1956). On the origin of cancer cells. Science *123*, 309-314.

91 Ward, P.S., and Thompson, C.B. (2012). Metabolic reprogramming: a cancer hallmark even warburg did not anticipate. Cancer Cell *21*, 297-308. 10.1016/j.ccr.2012.02.014.

92 Wojtovich, A.P., and Foster, T.H. (2014). Optogenetic control of ROS production. Redox Biol *2*, 368-376. 10.1016/j.redox.2014.01.019.

93 Xiang, K., Jendrossek, V., and Matschke, J. (2020). Oncometabolites and the response to radiotherapy. Radiat Oncol *15*, 197. 10.1186/s13014-020-01638-9.

94 Yang, M., Soga, T., and Pollard, P.J. (2013a). Oncometabolites: linking altered metabolism with cancer. J Clin Invest *123*, 3652-3658. 10.1172/JCI67228.

95 Yang, Y., He, J., Zhang, B., Zhang, Z., Jia, G., Liu, S., Wu, T., He, X., and Wang, N. (2021). SLC25A1 promotes tumor growth and survival by reprogramming energy metabolism in colorectal cancer. Cell Death Dis *12*, 1108. 10.1038/s41419-021-04411-2.

96 Yang, Y., Karakhanova, S., Hartwig, W., D'Haese, J.G., Philippov, P.P., Werner, J., and Bazhin, A.V. (2016). Mitochondria and Mitochondrial ROS in Cancer: Novel Targets for Anticancer Therapy. J Cell Physiol *231*, 2570-2581. 10.1002/jcp.25349.

97 Yang, Y., Lane, A.N., Ricketts, C.J., Sourbier, C., Wei, M.H., Shuch, B., Pike, L., Wu, M., Rouault, T.A., Boros, L.G., Fan, T.W., and Linehan, W.M. (2013b). Metabolic reprogramming for producing energy and reducing power in fumarate hydratase null cells from hereditary leiomyomatosis renal cell carcinoma. PLoS One *8*, e72179. 10.1371/journal.pone.0072179.

98 Zhang, D.X., Zhang, J.P., Hu, J.Y., and Huang, Y.S. (2016). The potential regulatory roles of NAD(+) and its metabolism in autophagy. Metabolism *65*, 454-462. 10.1016/j.metabol.2015.11.010.

99 Zhao, T., Mu, X., and You, Q. (2017). Succinate: An initiator in tumorigenesis and progression. Oncotarget *8*, 53819.

7 Attachments

7.1 Tables

7.2 Figures

7.3 Abbreviations

Acetyl-CoA	Acetyl coenzyme A
ATM	ataxia telangiectasia mutation
ATP	Adenosine triphosphate
BER	Base excision repair
CTPI2	Citrate transport protein inhibitor 2
D-2HG	D-2-hydroxyglutarate
DDR	DNA damage response
DHE	Dihydroethidium
DNA-PK(cs)	DNA dependent protein kinase (catalytic subunit)
DSB	Double strand break
EJ	end-joining
EMT	epithelial-to-mesenchymal transition
ETC	electron transport chain
FH	fumarate hydratase
Gy	Gray
h	hours
HCC	hepatocellular carcinoma
HIF	hypoxia-inducible factor
HLRCC	hereditary leiomyomatosis and renal cell cancer
HRR	Homologous recombination repair
HRness	Homologous recombination repair deficient
IDH	isocitrate dehydrogenase
IR	radiation (Ionizing radiation)

KDM	histone lysine demethylase
LDH	lactate dehydrogenase
MDH	malate dehydrogenase
NAD^+	Oxidized nicotinamide adenine dinucleotide
NADH	Reduced nicotinamide adenine dinucleotide
$NADP^+$	Oxidized nicotinamide adenine dinucleotide phosphate
NADPH	Reduced nicotinamide adenine dinucleotide phosphate
NHEJ	Non-homologous end joining
O_2	molecular Oxygen
OXPHOS	oxidative phosphorylation
PARP	Poly ADP-ribose polymerase
PARPi	PARP inhibitor
PBS	Phosphate-Buffered Saline
PI	Propidium iodide
PPP	pentose phosphate pathway
ROS	Reactive oxygen species
RT	Radiotherapy
SDH	Succinate dehydrogenase
SEM	Standard error of the mean
SF	Survival fraction
siRNA	small interfering ribonucleic acid
SLC25A1	solute carrier family 25 member 1
SSC	Side scatter light

SUCNR1	succinate receptor 1
TCA	tricarboxylic acid cycle
TET	ten eleven translocation DNA demethylase
VEGF	vascular endothelial growth factor
αKG	α-ketoglutarate,
αKGDD	α-ketoglutarate-dependent dioxygenase
γH2AX:	Histone H2AX phosphorylated at serine 139
e.g.	for example

8 Acknowledgements

First and foremost, I would like to show my deepest gratitude to my supervisor, Prof. Dr. rer. nat. Verena Jendrossek, a respectable, responsible and resourceful scholar, who offered me a precious opportunity to do scientific research in her laboratory and provided me with valuable guidance in every stage of the writing of my thesis.

I would like to gratefully acknowledge the enthusiastic supervision of Dr. rer. nat. Johann Matschke during the work. He has designed this project and given me guidance in experimental techniques and guided me throughout the whole process of my thesis.

I also thank Prof. Dr. rer. nat. Ulf Dittmer, Prof. Dr. rer. nat. Mengji Lu and Mrs. Ursula Schrammel of China cooperation office for helping me make my life abroad much easier and for their encouragement and support.

I appreciate Dr. rer. nat. Florian Wirsdörfer, Dr. rer. nat. Silvia Vega Rubin de Celis, Mrs. Angelika Warda, Mrs. Eva Gau, Mr. Mohamed Benchellal and Mrs. Ivonne Schulte for their help in my study.

I am thankful to my colleagues in our lab, who gave me a lot of help during my work, especially Safa Larafa, Isabell Götting, Mikhail Kunin, Katharina Eul, Sina Bader, Dr. rer. nat. Christine Hansel, Jetsy Karina Montero Vergara, Dr. rer. nat. Jennifer Steens, Alina Wittka for their kindly collaboration and well support in the experimental phase of my work.

Last but not least, I would like to thank my family. Their support and encouragement were ultimately what made this thesis possible. My family deserves my sincere gratitude and love for their dedication and support.

9 Curriculum vitae

The curriculum vitae is not included in the online version for data protection reasons